Bruker digital EPDIC luncheon

Welcome to our webinar today:

“Digital EPDIC luncheon”

We will start at 01:30 (CET)

Welcome to today's webinar from our Bruker AXS office in Karlsruhe, Germany!

Karsten Knorr
Product Manager
Industrial XRD

Martin Zimmermann
Product Manager
Thin-Film Analysis

Agenda – our EPDIC presentations

- In-operando characterization of $LiNi_XMn_yCo_zO_2$ pouch cells
- Joint PDF - Rietveld refinements of $LiMn_2O_4$ from laboratory data
- An efficient Rietveld compatible approach to (an)isotropic micro-strain broadening introduced by linearly correlated metric distributions
- Structural characterization of ultra-thin metallic films using coplanar and non-coplanar grazing incidence diffraction geometries
- Application of machine learning to XRD phase identification
- Q&A

In-operando Characterization of $LiNi_XMn_yCo_zO_2$ Pouch Cells

Dr. Christina Drathen
Product Manager XRD

Motivation

- Energy from renewable sources stored in batteries is a crucial building block for distributed electricity supply

- New cathode and anode materials are tested during charge- and discharge conditions

- XRD can directly monitor the compositional and structural changes
  - Structure of new cathode/ anode materials
  - In-situ studies of reactions during cycling

- Example: $LiNi_xMn_yCo_zO_2$ (NMC) a cathode material

Testing Batteries with XRD
Key Components – Transmission geometry

Versatile configuration
- Structure solution and refinement
- Non-ambient or in-situ experiments

Mo tube
- Higher penetration through metal foils in pouch cells with Mo
- XRD pattern compressed in 2θ: more peaks in same angular range

Focusing mirror
- Maximize intensity and best resolution in transmission

EIGER2 R 500K
- Large active detector area for rapid data collection in snapshot mode
- Suitable for all wavelengths (Cr-Ag)

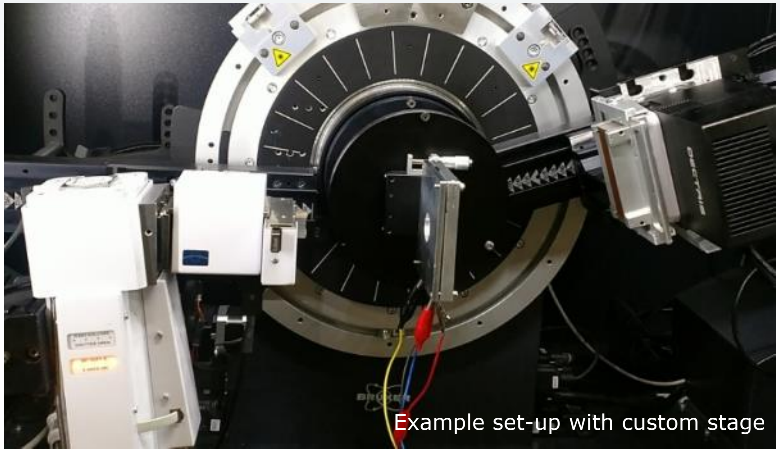
Example set-up with custom stage

Transmission set-up for in-situ studies	
Source	Mo sealed tube or TXS
Optic	Focusing Goebel mirror
Stage	Compact UMC or custom stage
Accessories	(UBC collimators) Panoramic Soller
Detector	EIGER2 R 500K

NMC Battery Pouch Cell

Charge/ Discharge cycles

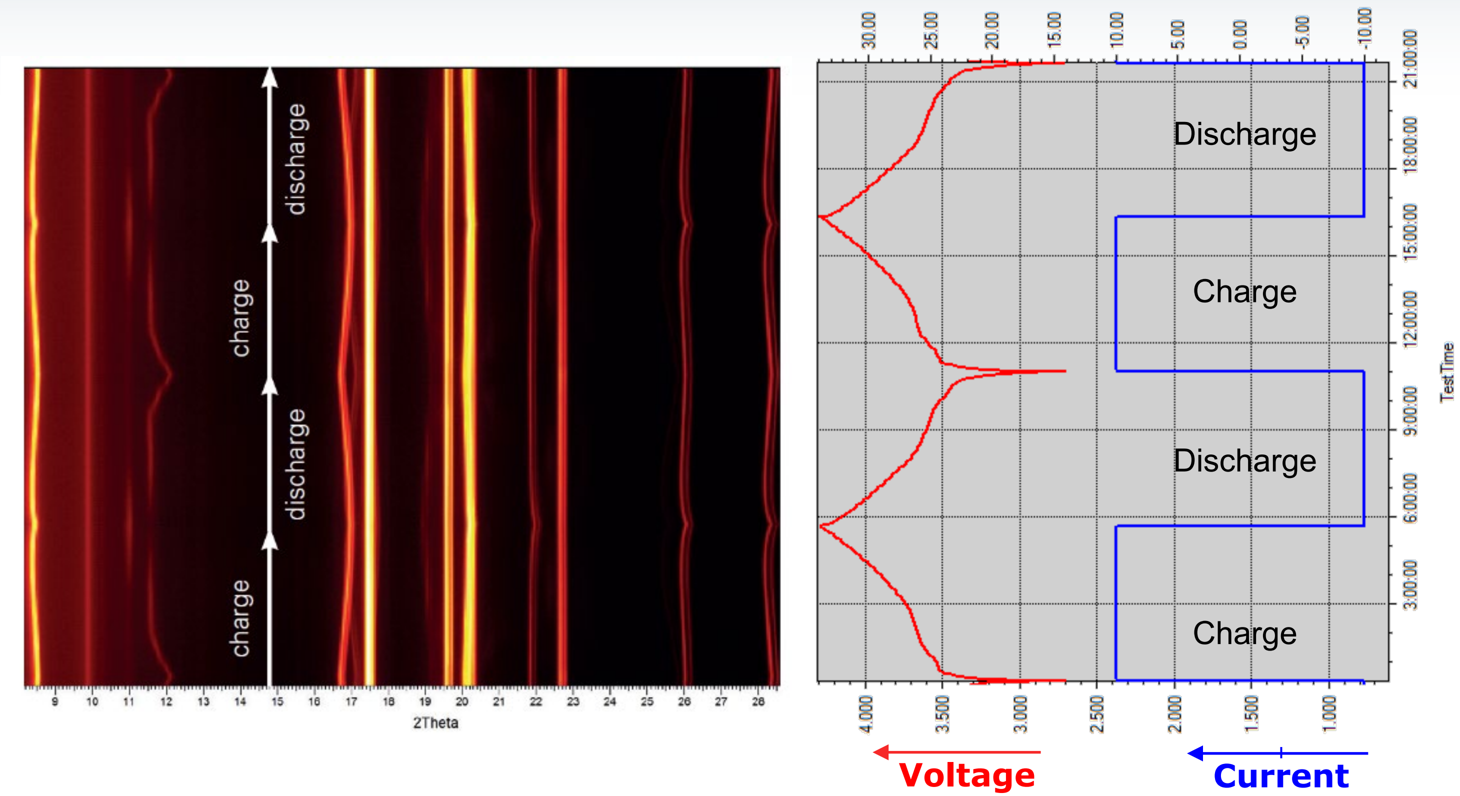

- Analysis of both anode and cathode
- Follow phase-composition and structural changes of NMC ($LiNi_xMn_yCo_zO_2$) battery with 3min data collection (7-32° 2θ) during C/5 charge/discharge conditions

NMC Battery Pouch Cell

Data visualization & analysis in DIFFRAC.EVA

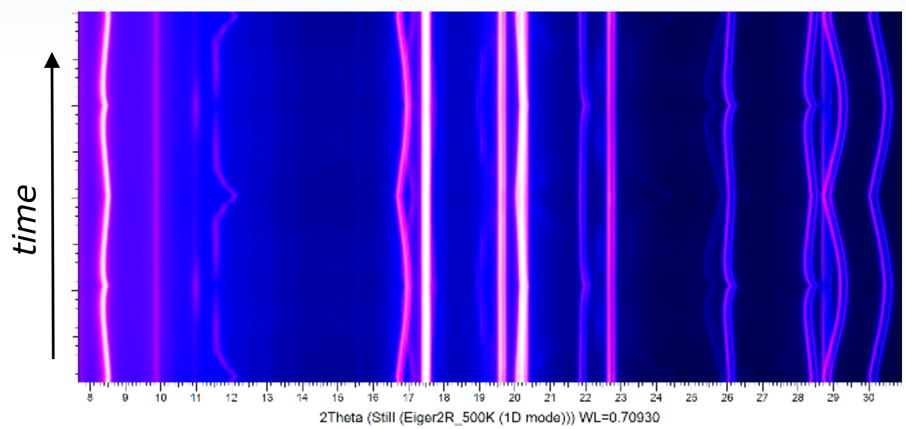

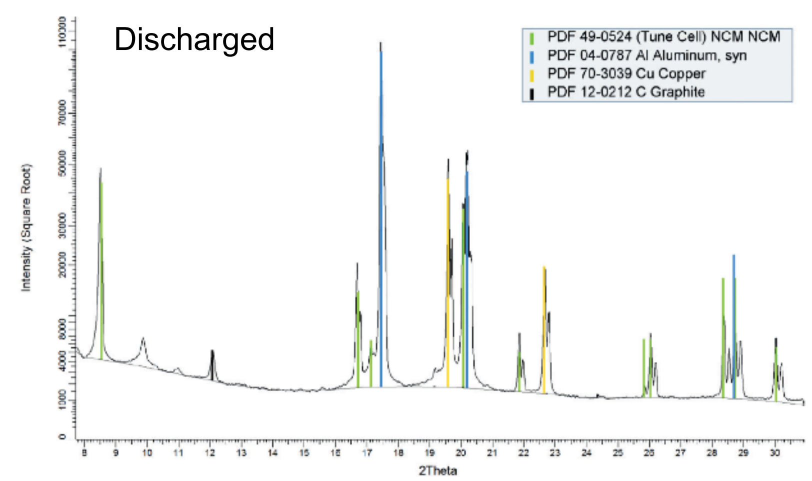

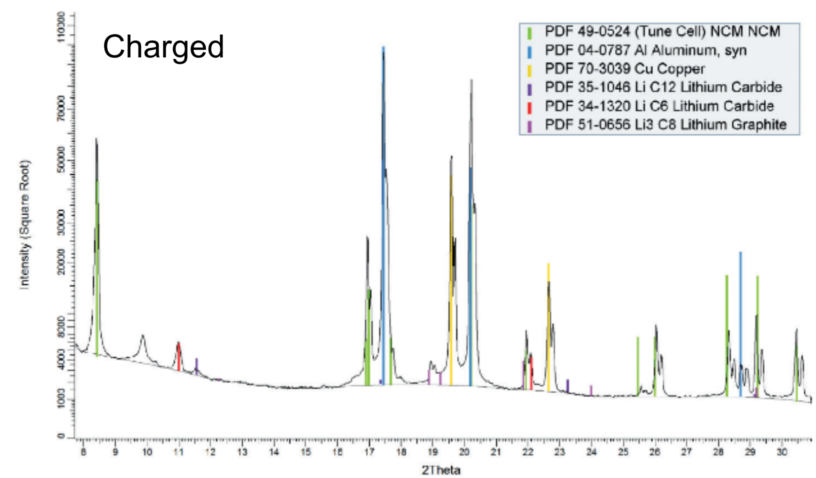

- Iso-intensity (2D) plots and Waterfall plots for data visualization
- Cluster analysis tools for identifying new phases during battery cycling
- Individual scans can be highlighted in the 2D plot and analyzed in more detail

NMC Battery Pouch Cell
Structure analysis in DIFFRAC.TOPAS

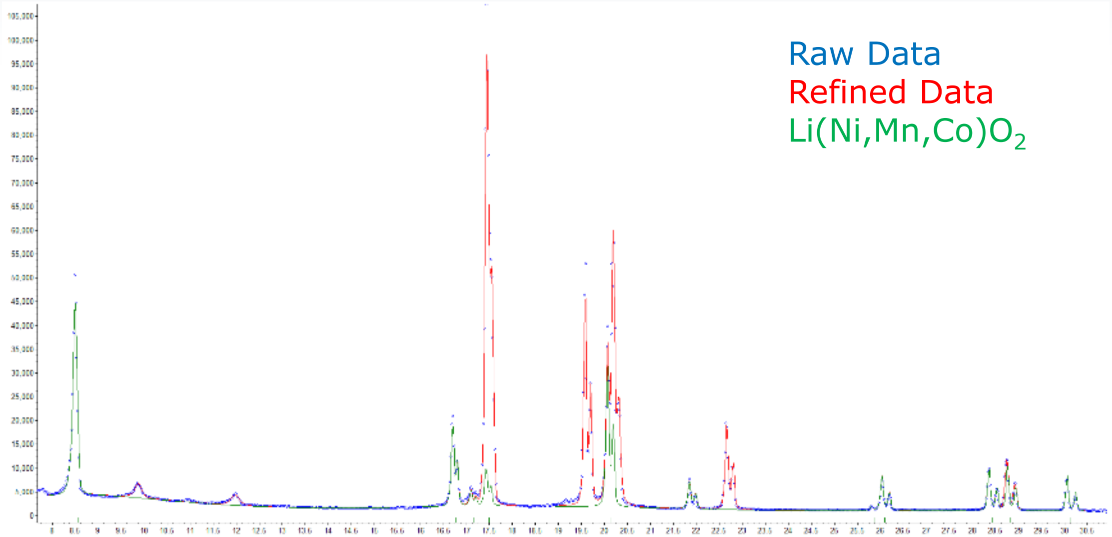

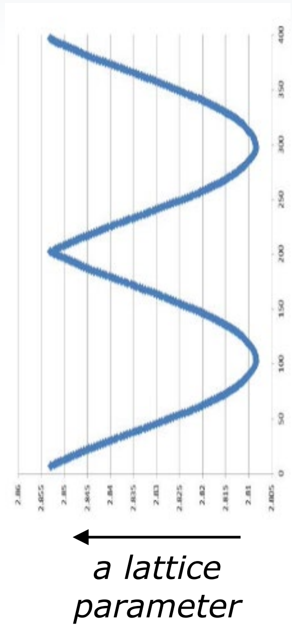

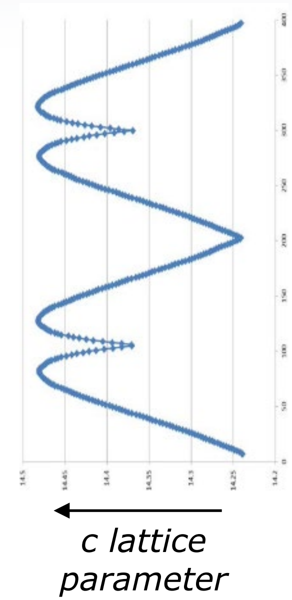

- Fast refinement of large datasets with customizable output of desired parameters using serial (batch) or parallel processing in TOPAS
- In thicker cells, different parts are at different positions → peak shift in XRD can be treated **correctly** in TOPAS[1]

[1] Rowles, M.R. & Buckley, C.E. (2017), J. Appl. Crys. 50, 240-251

What’s happening in the battery?
Anode

- Intercalation of Li in graphite:

  $Li + C \rightarrow LiC_x$ (x = 24, 12, 6)
- c-lattice parameter increases

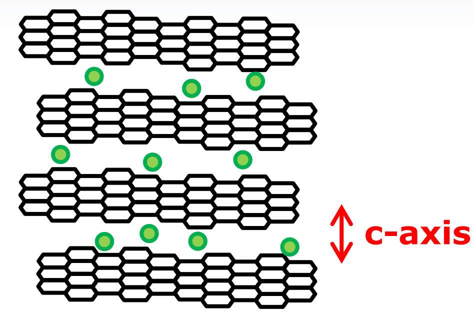

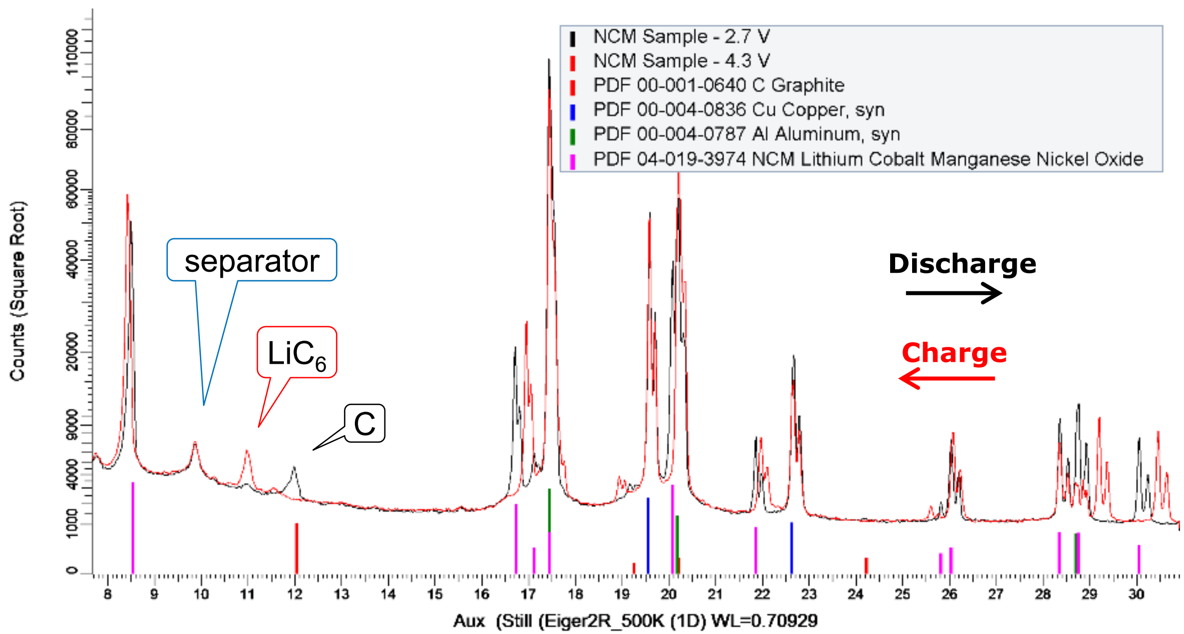

Graphite (002) reflection

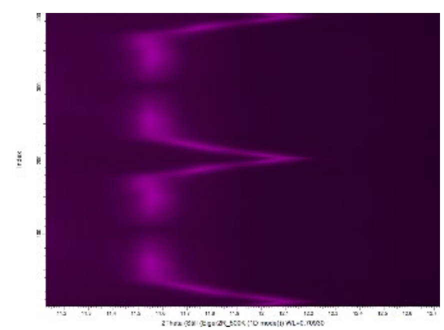

What's happening in the battery?
Cathode

- Li is removed from Li(NMC):

  $$LiNi_xMn_yCo_zO_2 \rightarrow Li + Ni_xMn_yCo_zO_2$$

- Oxidation of Ni^{2+} to Ni^{3+} → smaller radius; (contraction of *a*-axis)

- Higher charge of metal oxide layer → higher electrostatic repulsion (*c*-axis increases)

- At higher charge states (> 4V) possible charge-transfer from oxygen to metal → reduce electrostatic repulsion (*c*-axis decreases)

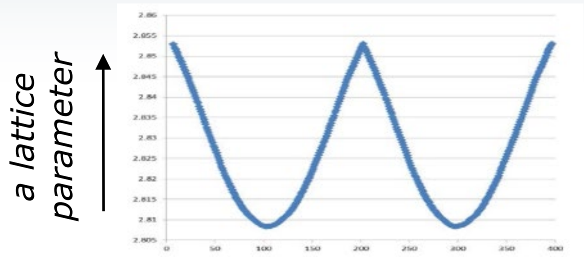

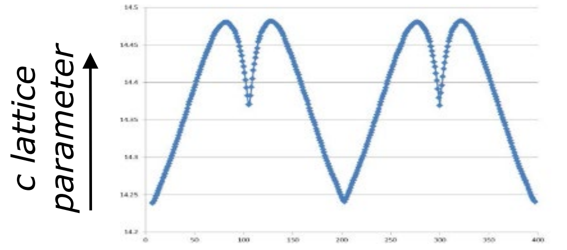

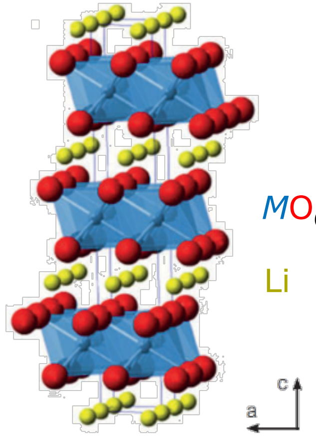

NMC Battery Pouch Cell
Summary

- Hard Mo-radiation to penetrate metal foils of pouch-cell and investigate entire battery at the same time
  - ✓ Diffraction pattern compressed (more peaks in same 2θ compared to Cu-radiation)
- Large EIGER2 R 500K detector for large 2θ coverage
  - ✓ Flexible positioning of detector increase 2θ range to 25º
- Large datasets are visualization rapidly in DIFFRAC.EVA.
  - ✓ EVA's clustering algorithms for efficient evaluation of hundreds or thousands of patterns.
- Correct description of geometrical effects (e.g. position of battery cell) with Rietveld analysis in DIFFRAC.TOPAS
  - ✓ Extremely fast serial and parallel refinements with 64bit version and multi-threading.

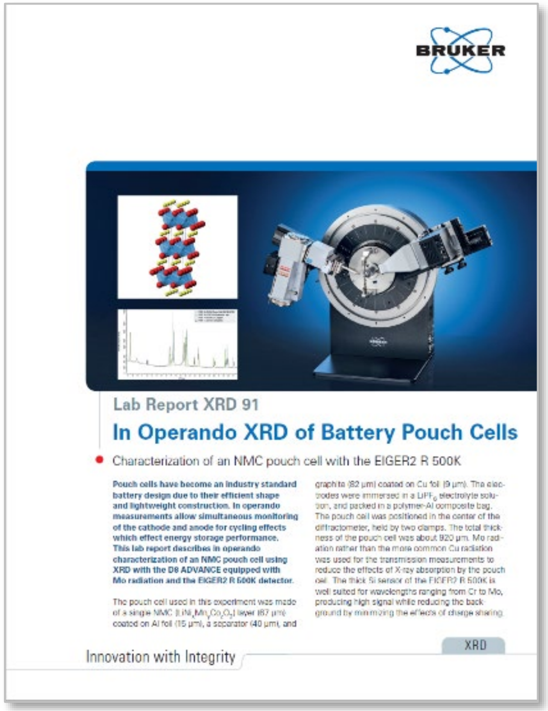
Lab Report XRD 91

In Operando XRD of Battery Pouch Cells

- Characterization of an NMC pouch cell with the EIGER2 R 500K

Pouch cells have become an industry standard battery design due to their efficient shape and lightweight construction. In operando measurements allow simultaneous monitoring of the cathode and anode for cycling effects which effect energy storage performance. This lab report describes in operando characterization of an NMC pouch cell using XRD with the D8 ADVANCE equipped with Mo radiation and the EIGER2 R 500K detector.

The pouch cell used in this experiment was made of a single NMC ($LiNi_xMn_yCo_zO_2$) layer (67 µm) coated on Al foil (15 µm), a separator (40 µm), and graphite (82 µm) coated on Cu foil (9 µm). The electrodes were immersed in a $LiPF_6$ electrolyte solution, and packed in a polymer-Al composite bag. The pouch cell was positioned in the center of the diffractometer, held by two clamps. The total thickness of the pouch cell was about 920 µm. Mo radiation rather than the more common Cu radiation was used for the transmission measurements to reduce the effects of X-ray absorption by the pouch cell. The thick Si sensor of the EIGER2 R 500K is well suited for wavelengths ranging from Cr to Mo, producing high signal while reducing the background by minimizing the effects of charge sharing.

XRD

Innovation with Integrity

Lab Report XRD 91

Joint PDF – Rietveld refinements of $LiMn_2O_4$ from laboratory data

Michael Evans
Application Scientist
XRD

Joint PDF-Rietveld refinements
Motivation

Problem

- $LiMn_2O_4$ is used as a cathode material
- Based on its stoichiometry and room temperature structure, average valence of $Mn^{3.5+}$
  - Physical properties, like electrical resistivity, do not fit this picture
- Local ordering of Mn^{3+} and Mn^{4+} ions at RT not visible in average structure?*

Solution

- Analyze structure across different length scales using Rietveld and PDF refinements
- Is there a convenient lab instrument to do this?

*Kodama, K. et al., J. Phys. Soc. Jpn. 82, 094601 (2013)

Why joint Rietveld-PDF refinements?
Average vs. local structure

Si-O bond in α-quartz

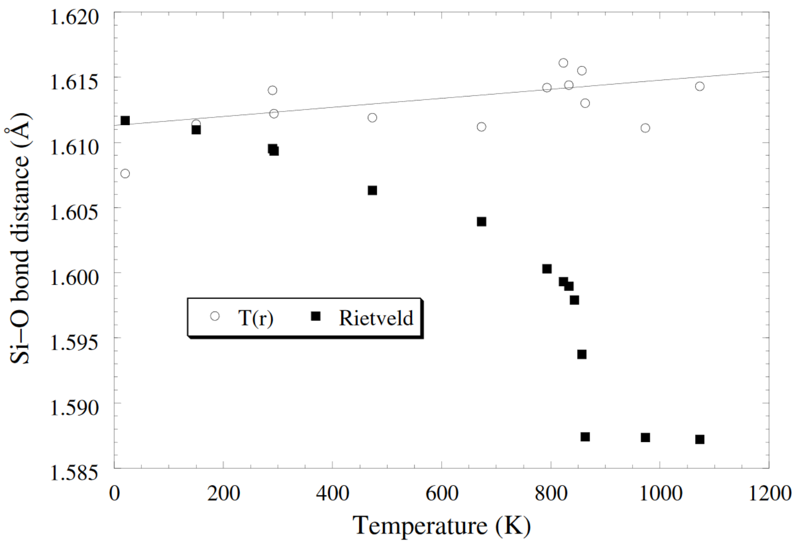

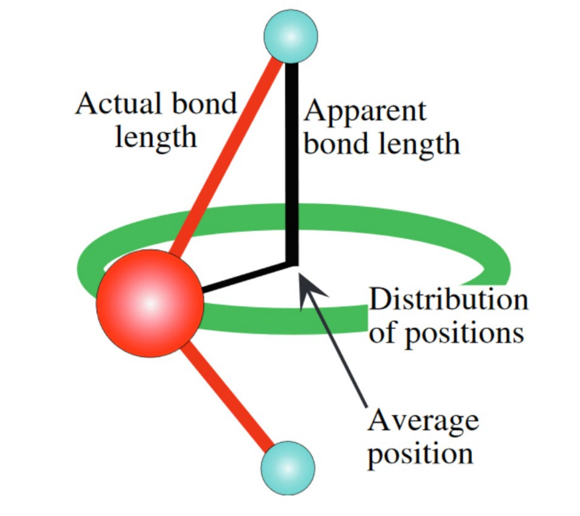

- **Classic diffraction**
  Distance between averaged positions of pairs of atoms
- **Pair Distribution Function**
  Average distance between pairs of atoms

M.G. Tucker, D.A. Keen and M.T. Dove; Miner. Mag. **65** (2001) 489-507
M.G. Tucker, M.T. Dove and D.A. Keen; J. Phys.: Condens. Matter **12** (2000) L425-L430

Joint PDF-Rietveld Refinements

Key Components – Transmission geometry

Versatile configuration

- Structure solution and refinement
- Non-ambient or in-situ experiments

Mo source

- Higher accessible Q range necessary for PDF measurements
- Higher d-space resolution for structure refinement

Focusing Goebel mirror

- Maximize intensity and high resolution in transmission

EIGER2 R 500K

- Large active detector area for faster data collection and best statistics
- Suitable for all wavelengths (Cr-Ag)

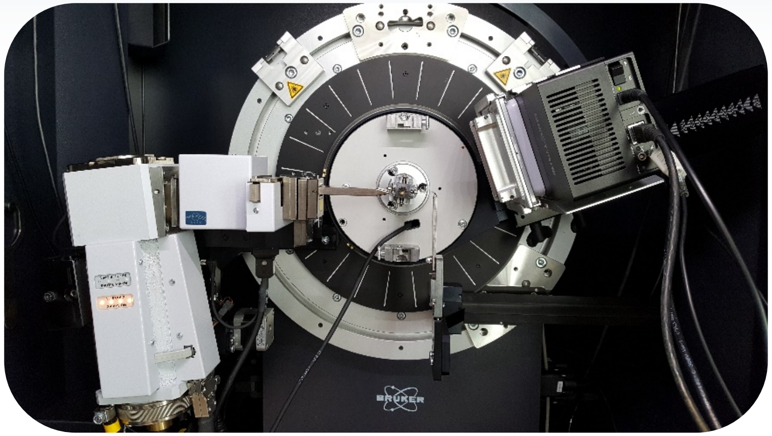

Configuration for joint refinements	
Source	Mo sealed tube
Optic	Focusing Goebel mirror
Stage	Capillary stage
Accessories	UBC scatter guard Beam stop Panoramic Soller
Detector	EIGER2 R 500K
Collection time	**75 min**

Cathode Material $LiMn_2O_4$
Rietveld Analysis at RT

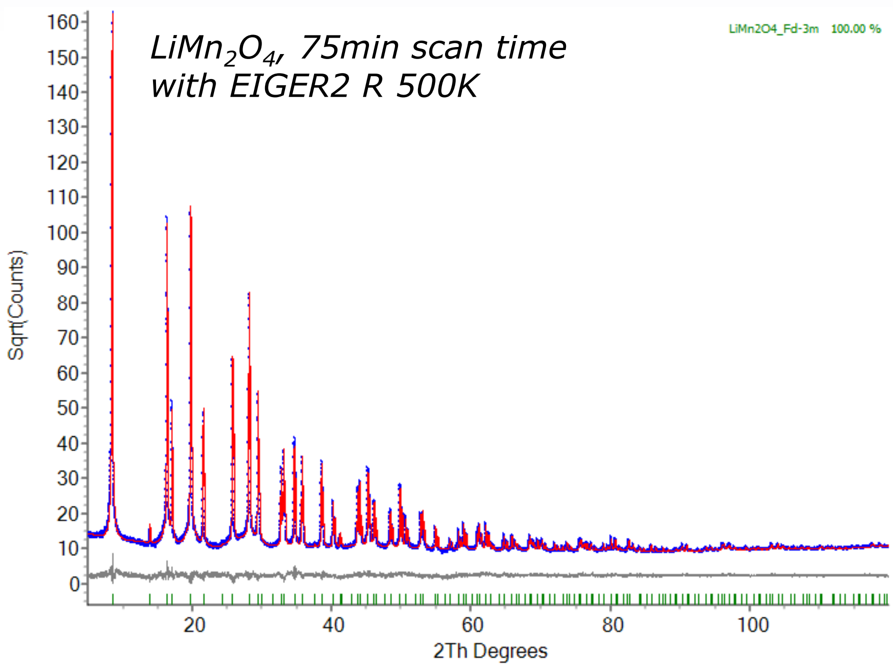

Atom	x	y	z	B (Å²)
Li	1/8	1/8	1/8	1.55(9)
Mn	1/2	1/2	1/2	0.688(5)
O	0.2641(1)	0.2641	0.2641	1.49(2)

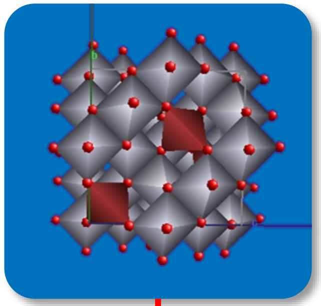

Room Temperature

- Cubic *Fd-3m*
- Average valence $Mn^{3.5+}$
- 6 equivalent Mn-O bonds = 1.951 Å

260 K

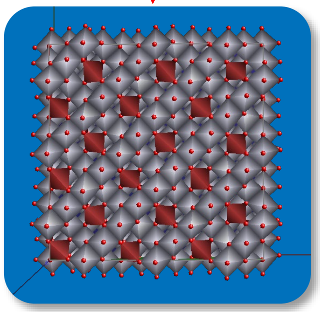

Low Temperature

- Orthorhombic *Fddd*
- Mn^{3+}/Mn^{4+} ordering
- Mn-O bonds between 1.82 to 2.23 Å
- Superlattice reflections, ($3a \times 3a \times a$) cell

Cathode Material $LiMn_2O_4$

Local Structure at RT

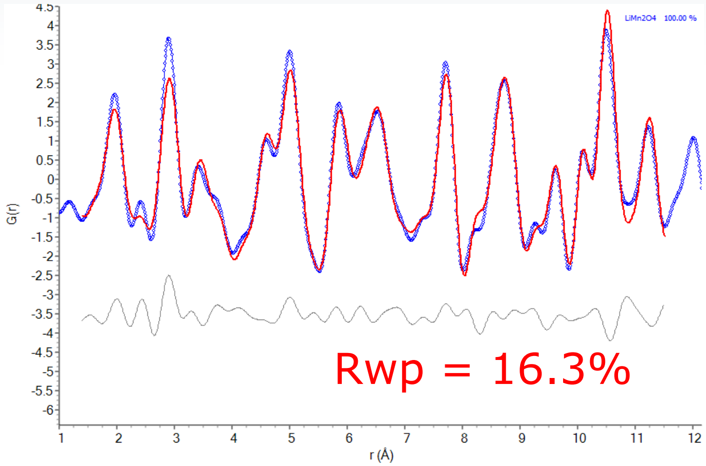

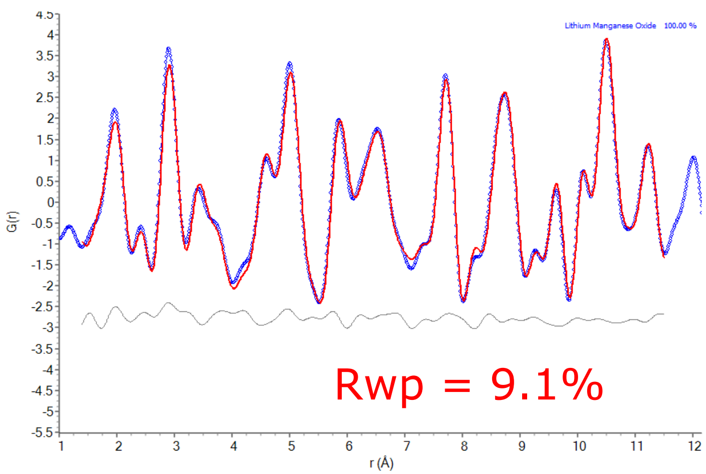

Cubic Fd-3m – disordered $Mn^{3.5+}$

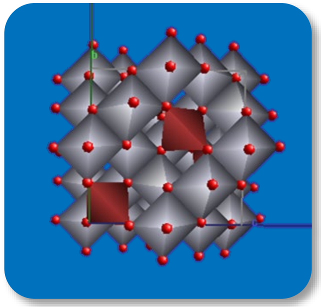

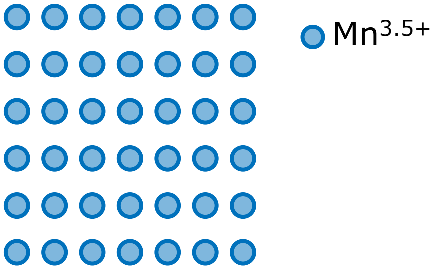

Mn-O bonds: 1.951 Å

Orthorhombic Fddd – ordered Mn^{3+}/ Mn^{4+}

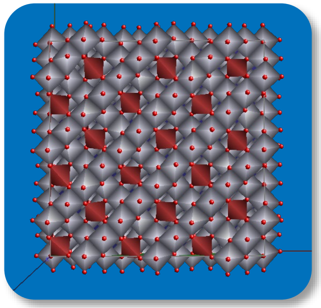

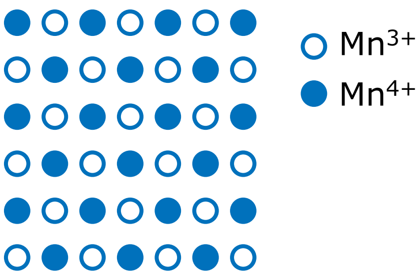

Mn-O bonds: 1.82 – 2.28 Å

Cathode Material $LiMn_2O_4$

Local Structure at RT

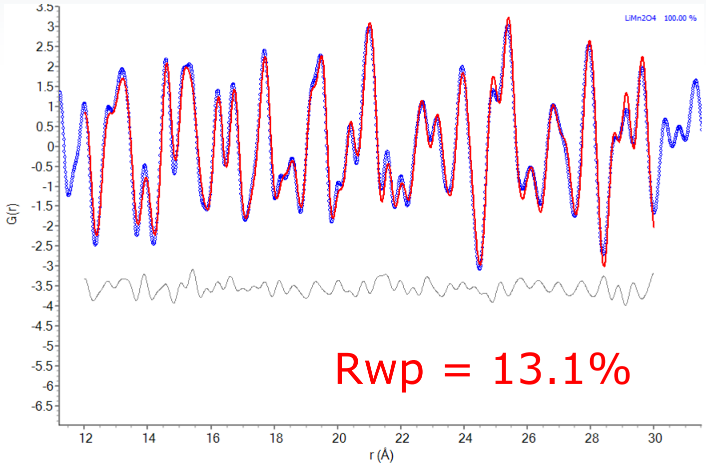

Cubic Fd-3m – disordered $Mn^{3.5+}$ on long range

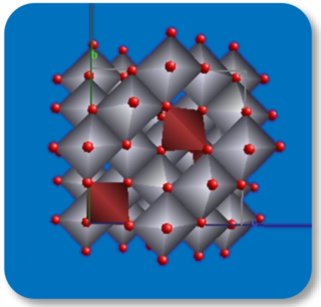

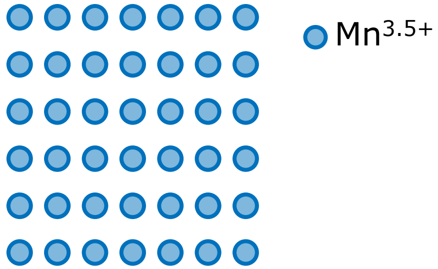

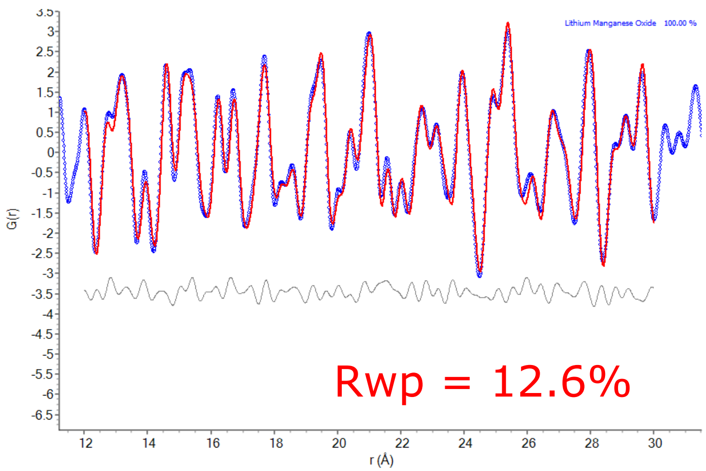

Orthorhombic Fddd - ordered Mn^{3+}/ Mn^{4+} domains

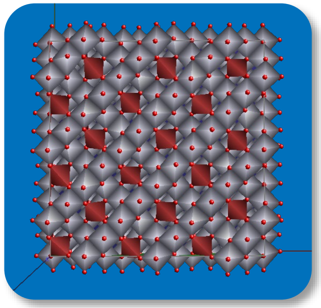

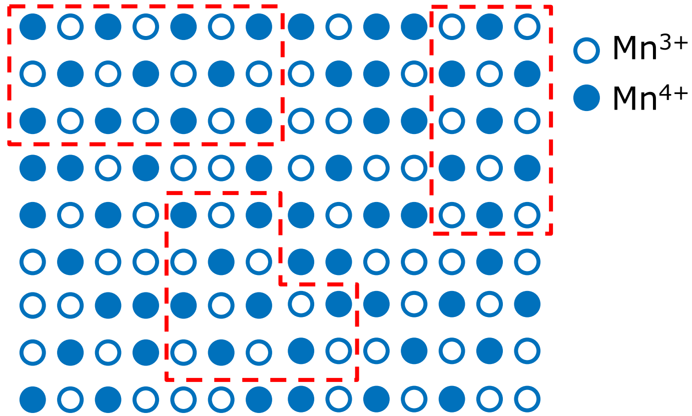

Box Car Refinement
Modelling over various r-range

- Box-car refinements: fixed length box and performing sequential refinements from low to high r-ranges
  - PDF fit to the cubic model gets better at higher r-range → closer to average structure

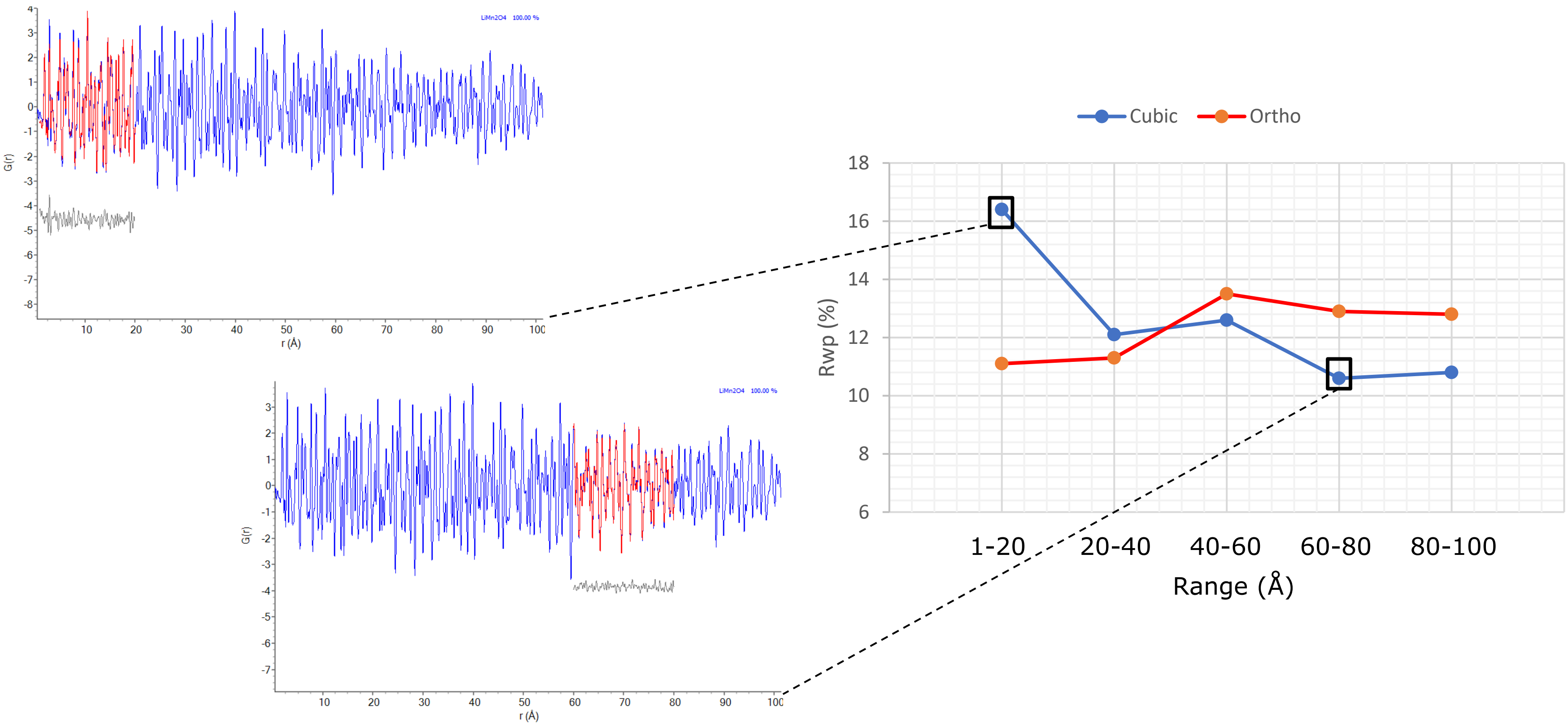

Hard Radiation Applications
Summary

- D8 ADVANCE with Mo source and EIGER2 R 500K is a versatile solution for many applications
- Hard radiation (Mo)
  - Larger accessible Q-space data for PDF analysis
  - Higher penetration into heavier materials
- Large EIGER2 R 500K detector
  - Large 2theta coverage ideal for monitoring changes in battery cells
  - Fast data collection
- Joint PDF-Rietveld refinements with DIFFRAC.TOPAS for investigations at different length scales

Battery Cells

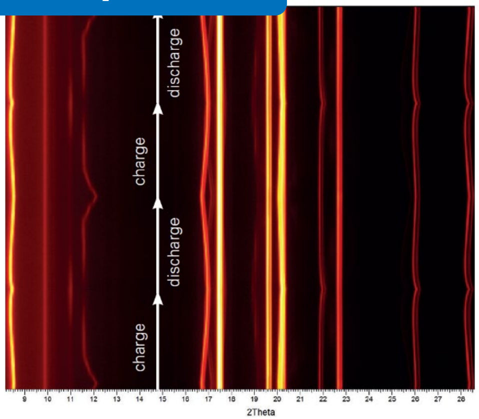

Rietveld and PDF refinements

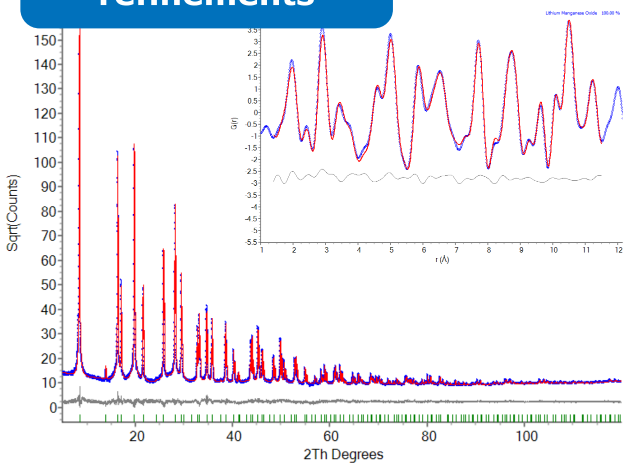

What’s new in XRD

EIGER2 R 500K for the D8 Family

One detector for all applications

Available as an upgrade for D8 ADVANCE and D8 DISCOVER

Key benefits of EIGER2

- Leading Sensor Design
- Dynamic Detector Optimization
- Solution level integration into DIFFRAC.SUITE

EIGER2 for the D8 Family
Leading Sensor Design

Outstanding Active Area
- 77.2 mm x 38.6 mm
- >529,000 pixels of 75 µm size
- Panoramic Optics for full Field-Of-View

Highest Dynamic Range
- Ultra-high count rate (3.6×10^8 cps/mm²)
- Dual threshold for lowest background

Compatible with Cr-Ag Radiation
- Covers the full range of applications from Stress analysis (Cr) over In-Operando Battery Analysis (Mo) to Pair Distribution Function (Ag)

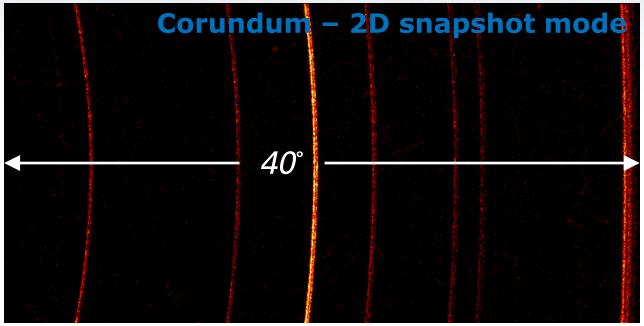

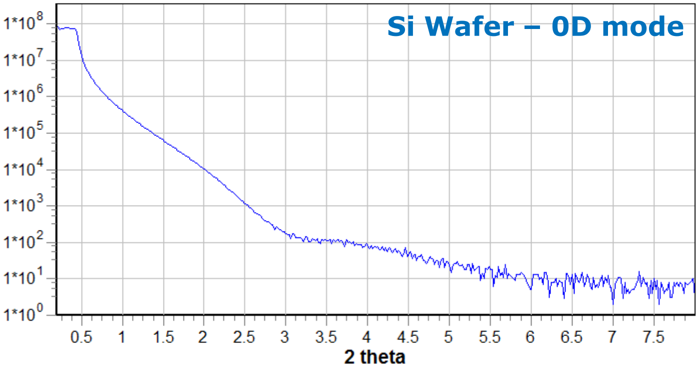

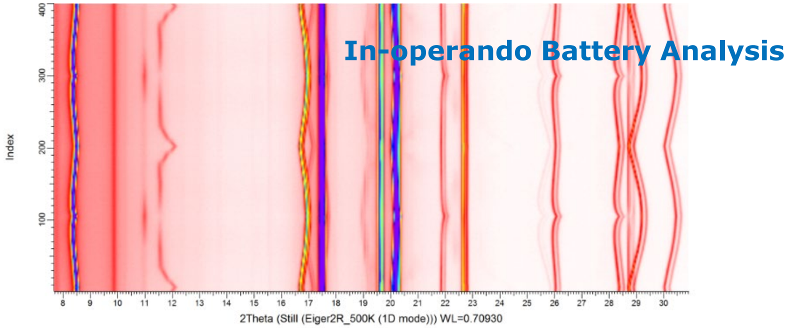

EIGER2 for the D8 Family
Dynamic Detector Optimization

Tool and Alignment-free
Coverage Adjustment

- Sample to detector distance
  - Continuously variable
- Detector orientation
  - 2θ or Gamma optimized
- D8 DISCOVER: Automated Distance Detection & Calibration

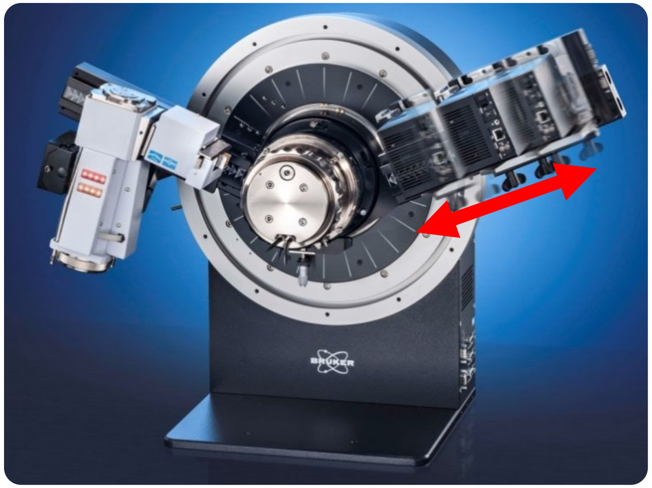

Seamless Software Integration

- Push-button detector mode selection
- Region of Interest (ROI) definition

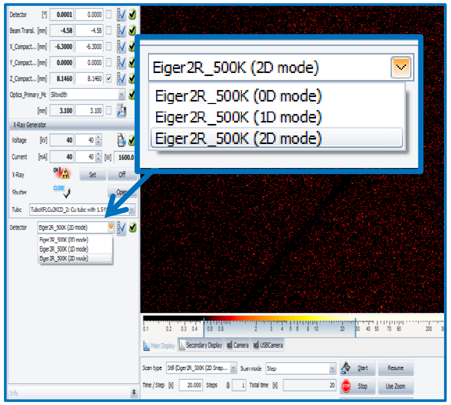

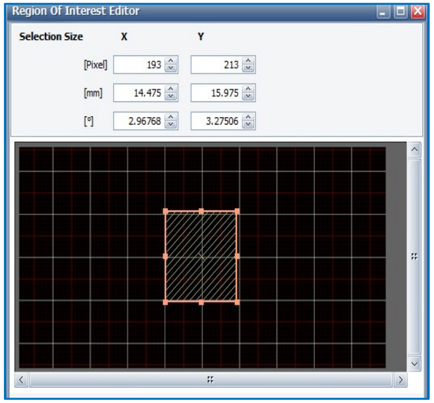

EIGER2 R 500K for D8 Family
Full integration into DIFFRAC.SUITE

Plan

- Real time recognition in **DAVINCI**
- **WIZARD** for Method Creation

Measure

- Push Button execution in **START JOBS**
- **COMMANDER** for measurement flexibility

Analyze

- 0D, 1D and <u>native</u> 2D data evaluation

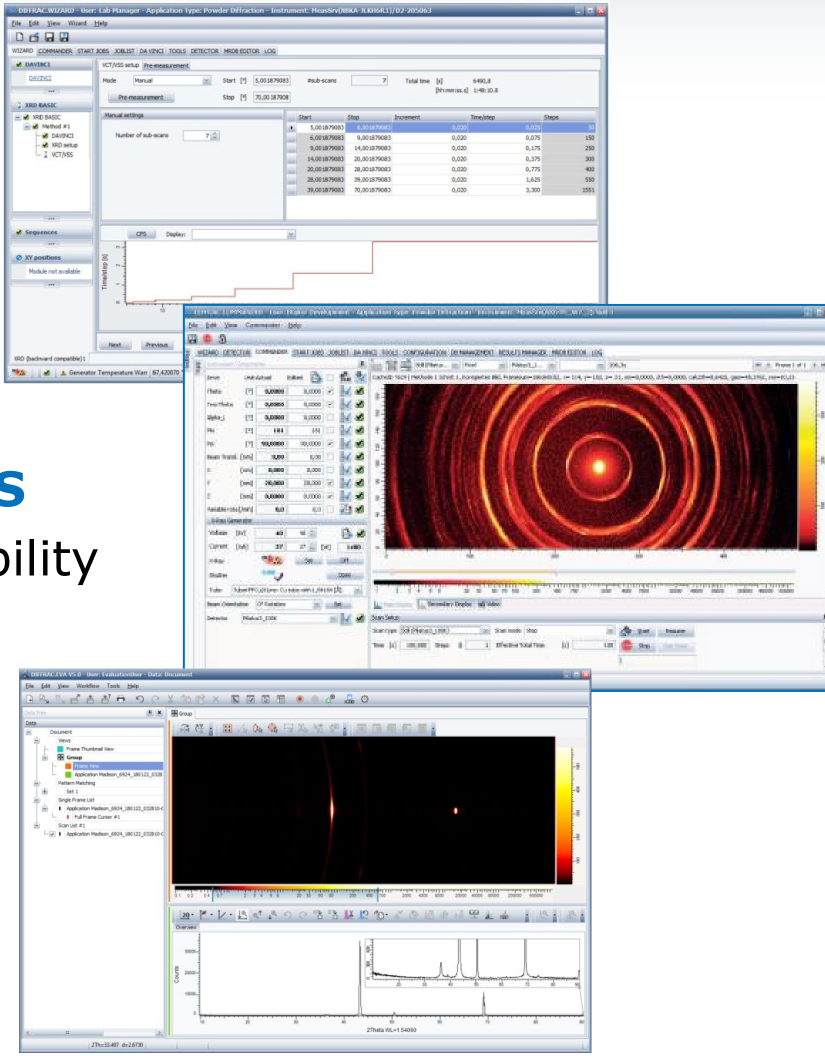

EIGER2 R 500K Upgrade for D8 Family
Summary

- Market leading EIGER2 is available as upgrade package for your D8 ADVANCE and D8 DISCOVER.
- The EIGER2 will expand your application range significantly, makes your work easier and faster.
- For further information please contact your local Bruker AXS representative or contact us at

info.BAXS@bruker.com

An efficient Rietveld compatible approach to (an)isotropic microstain broadening introduced by linearly correlated metric distributions

Dominique Ectors
Application Scientist
XRD

The problem – Anisotropic line broadening

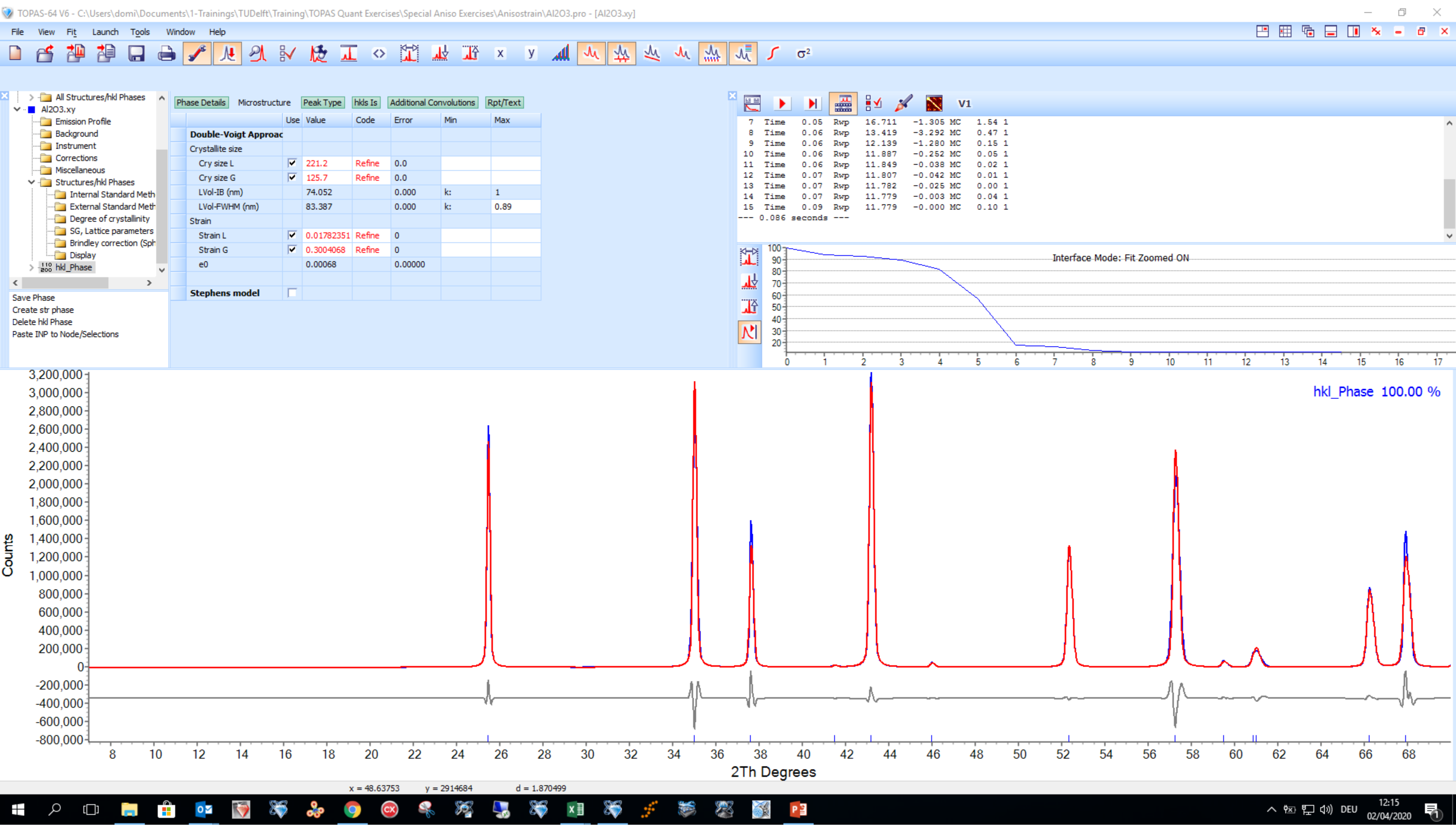

A popular solution – Stephens model

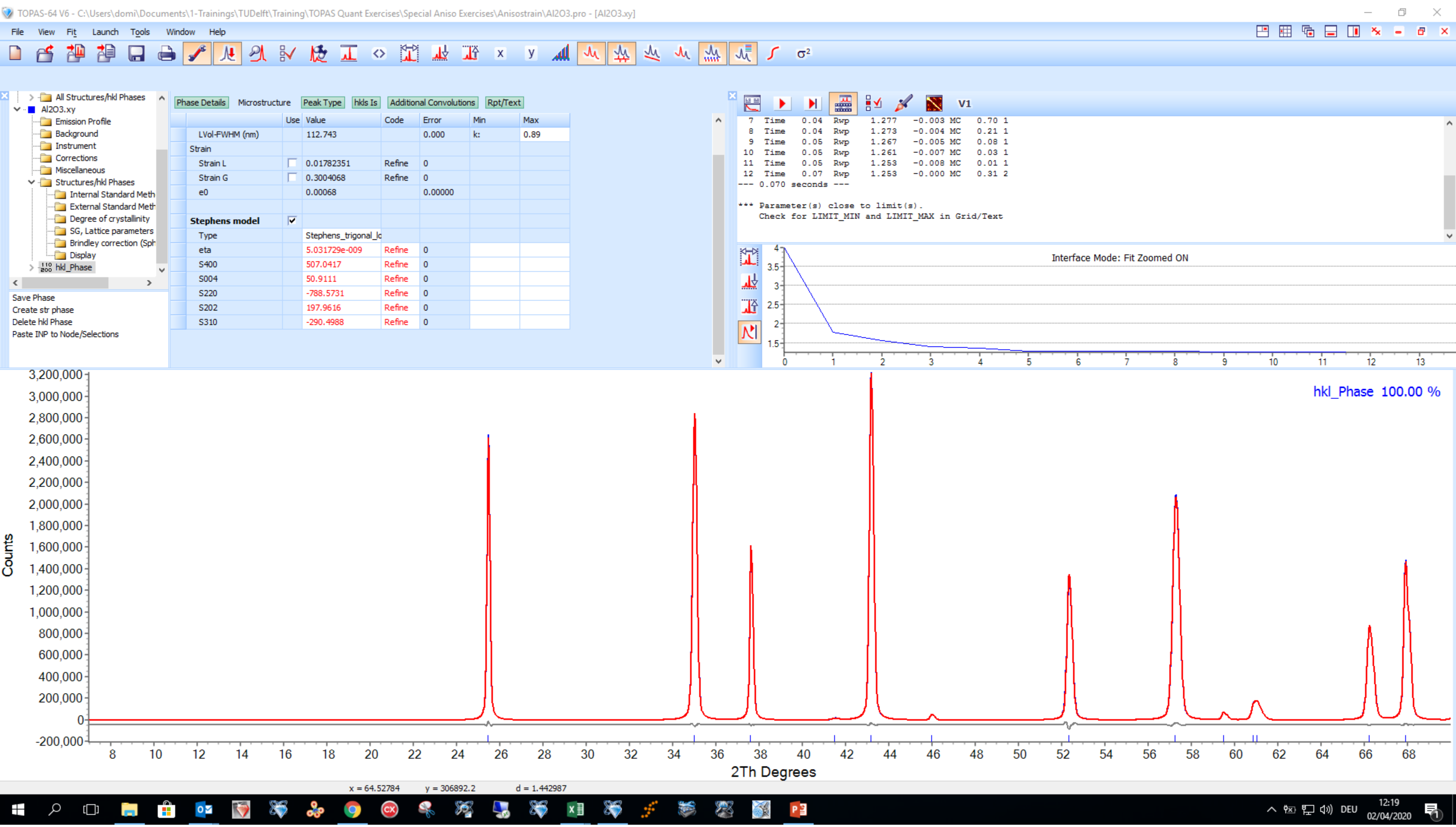

Stephens model – Yes but what does this mean ?

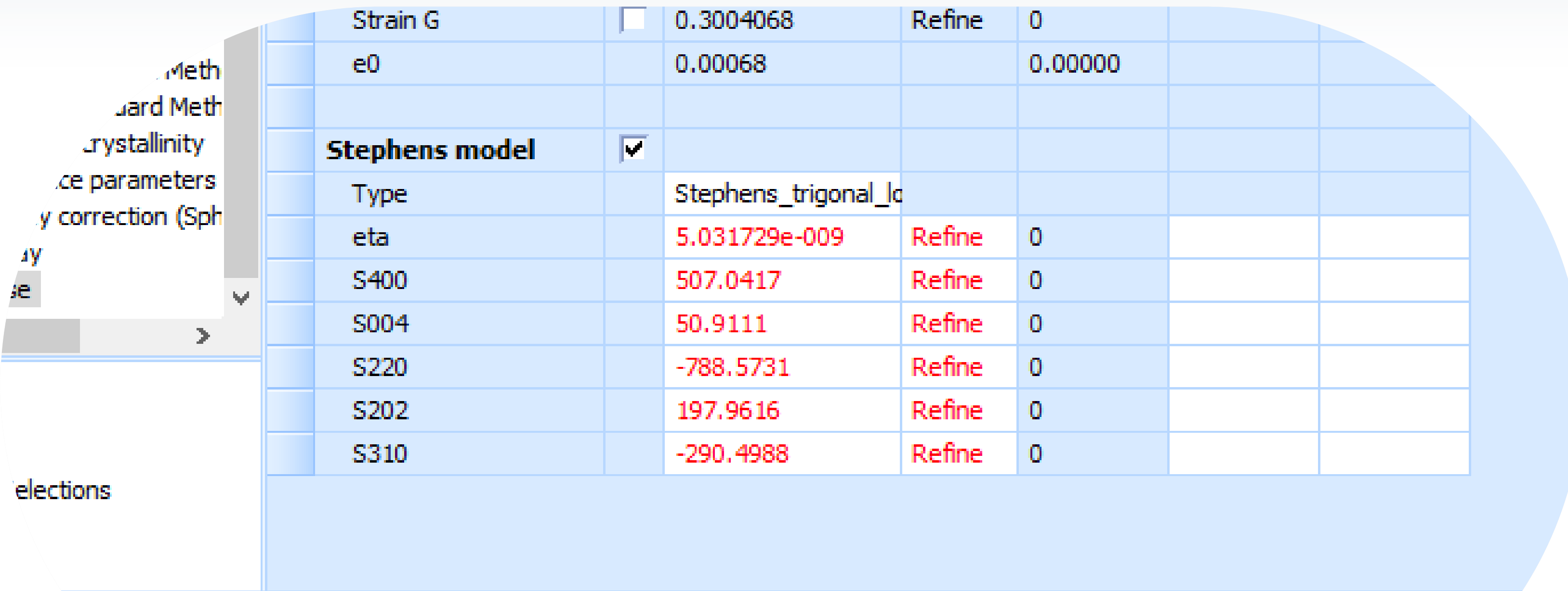

Strain G	☐	0.3004068	Refine	0		
e0		0.00068		0.00000		
Stephens model	☑					
Type		Stephens_trigonal_lc				
eta		5.031729e-009	Refine	0		
S400		507.0417	Refine	0		
S004		50.9111	Refine	0		
S220		-788.5731	Refine	0		
S202		197.9616	Refine	0		
S310		-290.4988	Refine	0		

The idea

- *Stephens (J. Appl. Cryst. (1999))*
  - *Multivariate distribution of reciprocal metric tensor values.*

$$\mathbf{G}^* = \begin{pmatrix} \mathbf{a}^* \cdot \mathbf{a}^* & \mathbf{a}^* \cdot \mathbf{b}^* & \mathbf{a}^* \cdot \mathbf{c}^* \\ \mathbf{b}^* \cdot \mathbf{a}^* & \mathbf{b}^* \cdot \mathbf{b}^* & \mathbf{b}^* \cdot \mathbf{c}^* \\ \mathbf{c}^* \cdot \mathbf{a}^* & \mathbf{c}^* \cdot \mathbf{b}^* & \mathbf{c}^* \cdot \mathbf{c}^* \end{pmatrix} = \begin{pmatrix} a^{*2} & a^* b^* \cos\gamma^* & a^* c^* \cos\beta^* \\ b^* a^* \cos\gamma^* & b^{*2} & b^* c^* \cos\alpha^* \\ c^* a^* \cos\beta^* & c^* b^* \cos\alpha^* & c^{*2} \end{pmatrix}$$

    - *Problem interpretation is not easy, will depend also on the absolute values of the reciprocal lattice parameters / Different parametrization approaches see Leineweber (2011) Z. Kristallogr. 226 905-923*

- *Let start with something simpler*
  - *Distribution of real or reciprocal lattice parameters*
    - *Relative deviations from the average lattice parameters as refinement parameters*

How it works, in essence

For a symmetric distribution we can define the microstrain as

$$e_{50\_X} = \left|\frac{\Delta d_X}{d_{0\_X}}\right| = \left|\frac{d_{Strain\_X} - d_{0\_X}}{d_{0\_X}}\right|$$

d0 for each HKL-Vector X is

$$d_{0\_X} = \sqrt{\boldsymbol{X^T} * \boldsymbol{G_0^*} * \boldsymbol{X}}^{-1}$$

dstrain for each HKL-Vector X is

$$d_{Strain\_X} = \sqrt{\boldsymbol{X^T} * \boldsymbol{G_{Strain}^*} * \boldsymbol{X}}^{-1}$$

The reciprocal metric tensor is calculated from the refinable parameters δa, δb, δc, $\delta\alpha$, $\delta\beta$, $\delta\gamma$. So e.g.

$$a_{Strain} = a_0 * \Delta a = a_0 * (1 + \delta a)$$

Anisotropic strain broadening & Lattice parameters

a=3Å
b=4Å
c=5Å±0.1‰

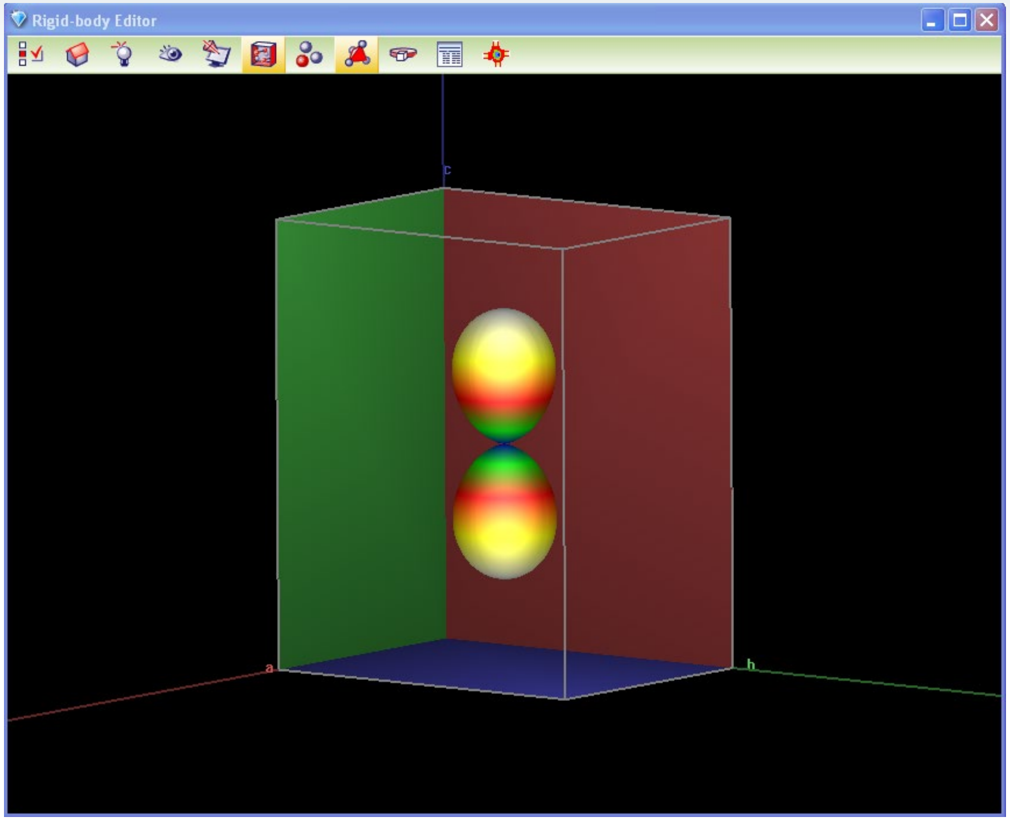

Anisotropic strain broadening & Lattice parameters

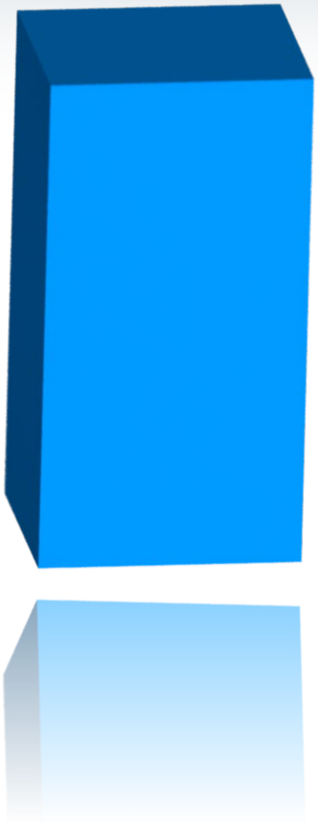

$a = 3$Å
$b = 4$Å± 0.1‰
$c = 5$Å± 0.1‰

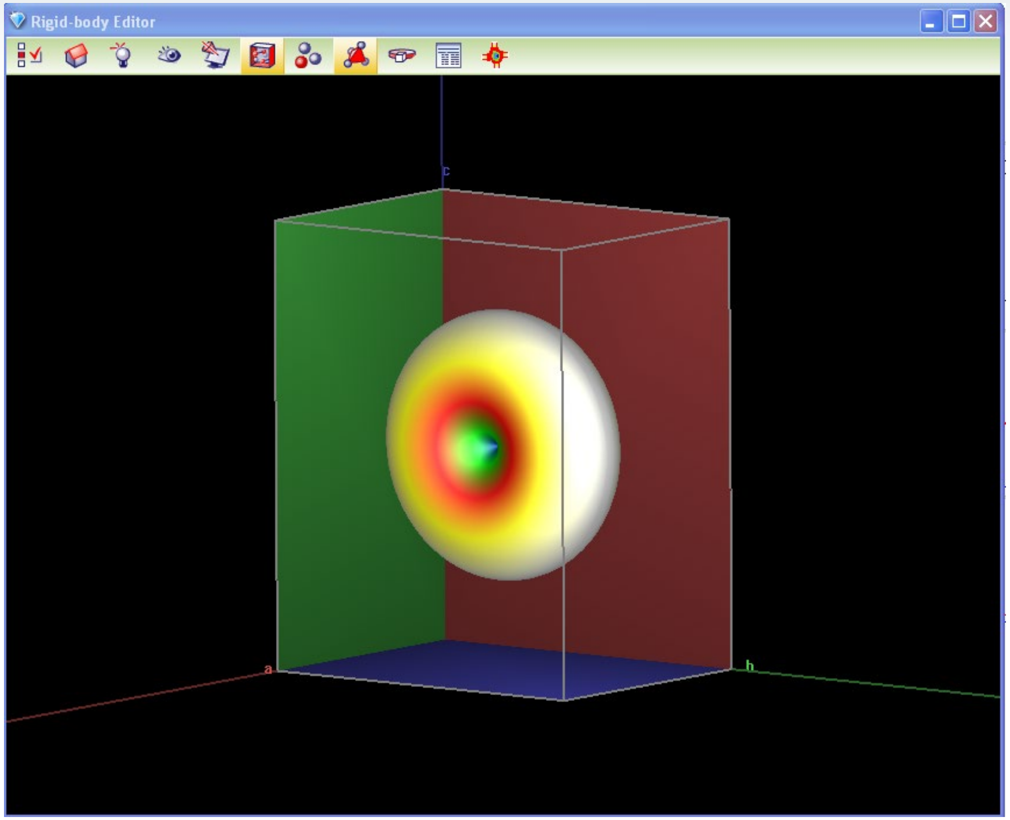

Anisotropic strain broadening & Lattice parameters

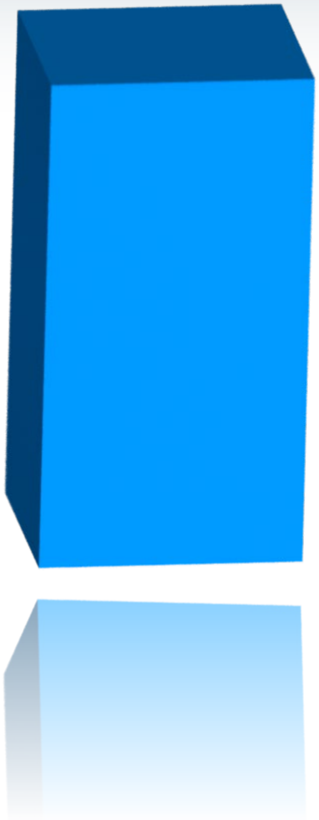

a=3Å∓0.1‰
b=4Å
c=5Å±0.1‰

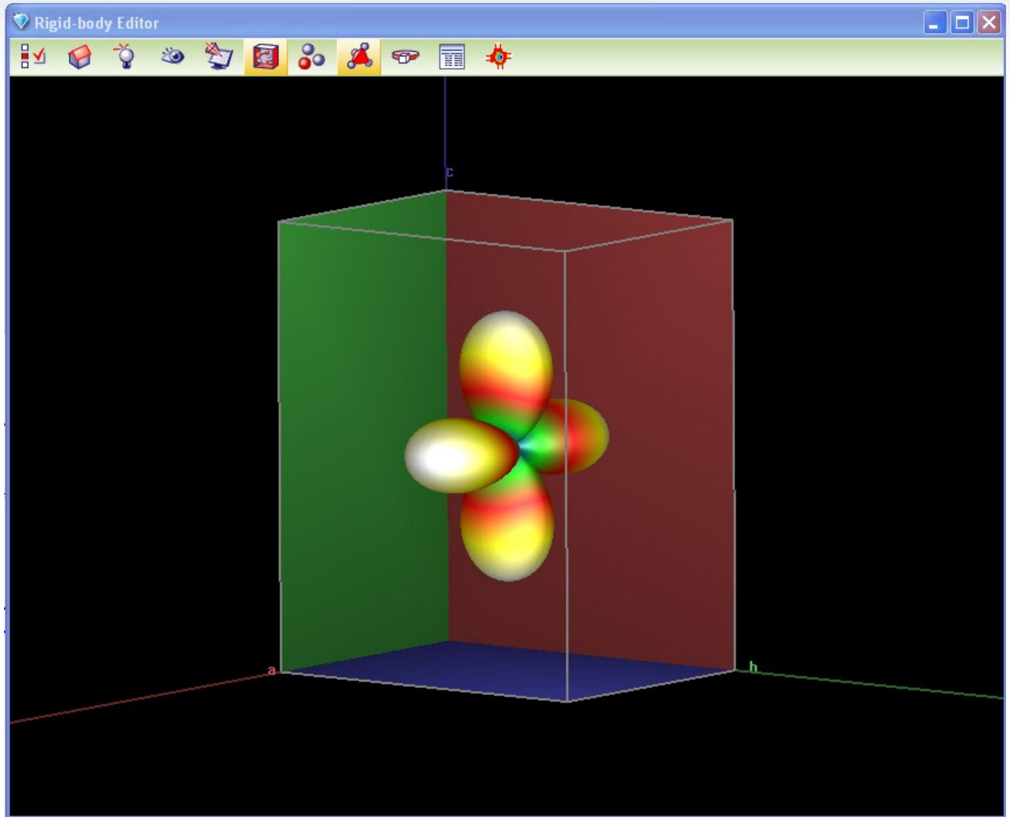

Anisotropic strain broadening & Lattice parameters

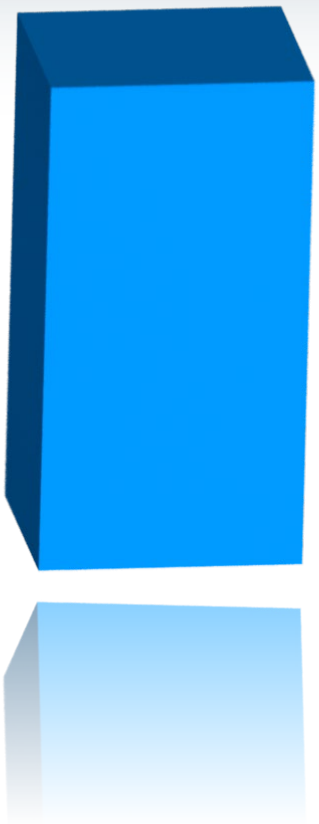

a=3Å∓0.1‰
b=4Å±0.1‰
c=5Å±0.1‰

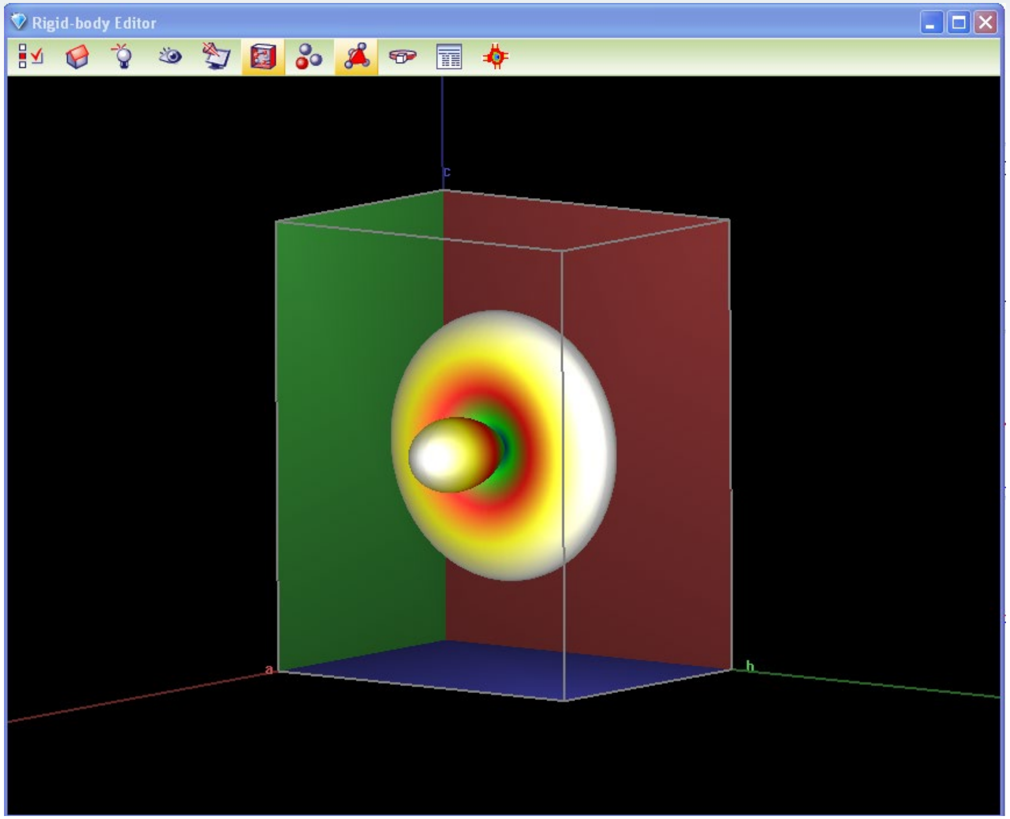

Anisotropic strain broadening & Lattice parameters

a=3Å
b=4Å
c=5Å
$\alpha=90\pm0.1$‰

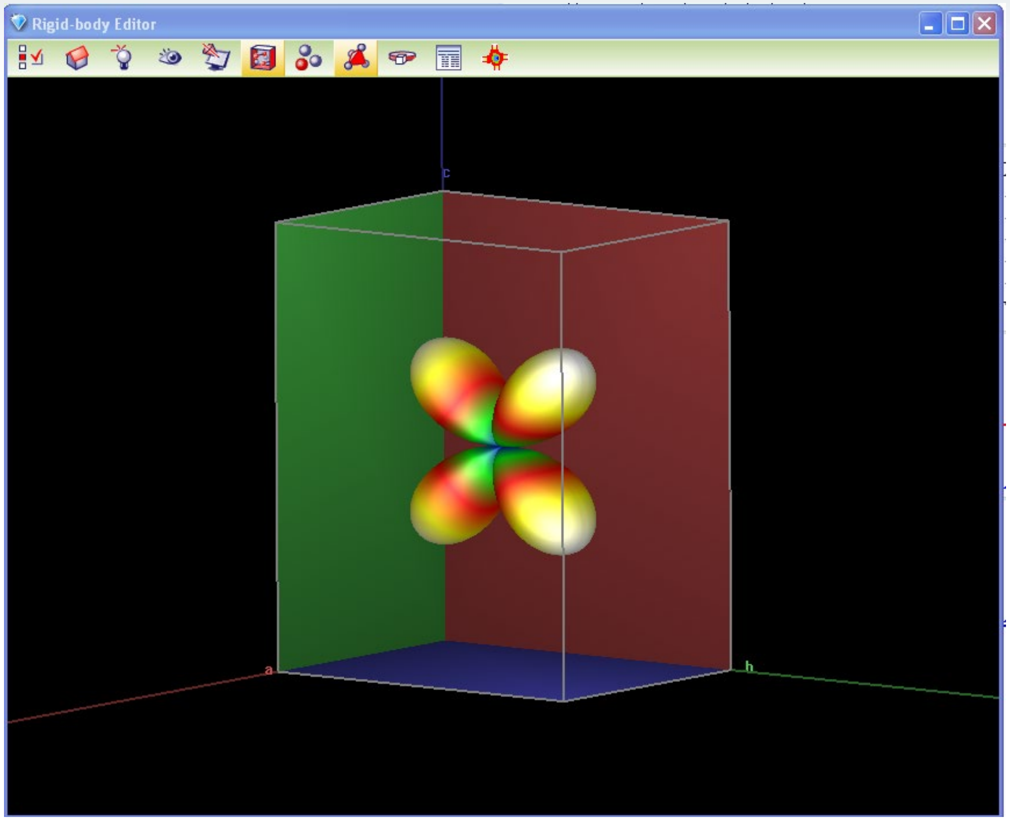

A popular solution – Stephens model

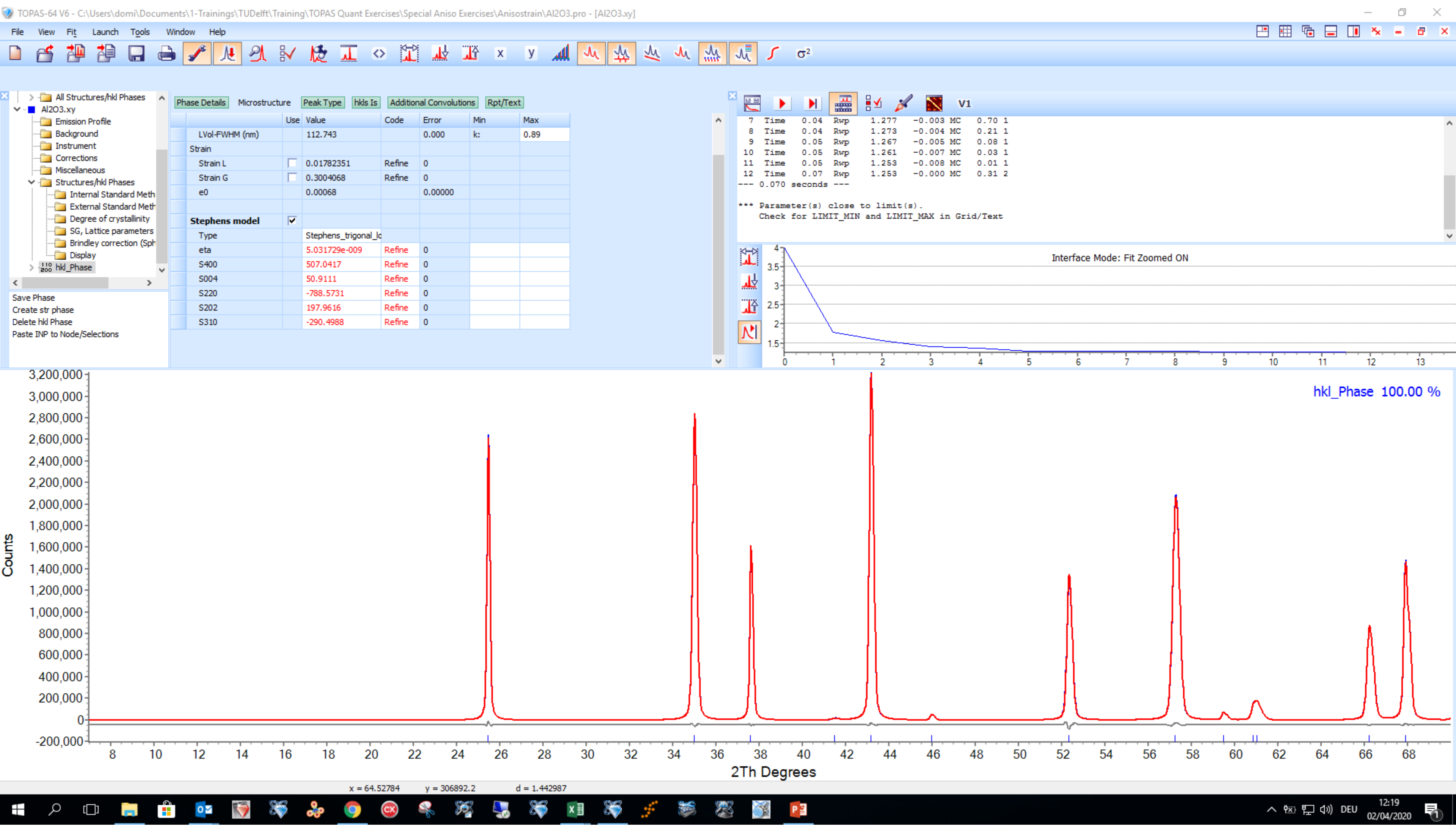

Proposed model

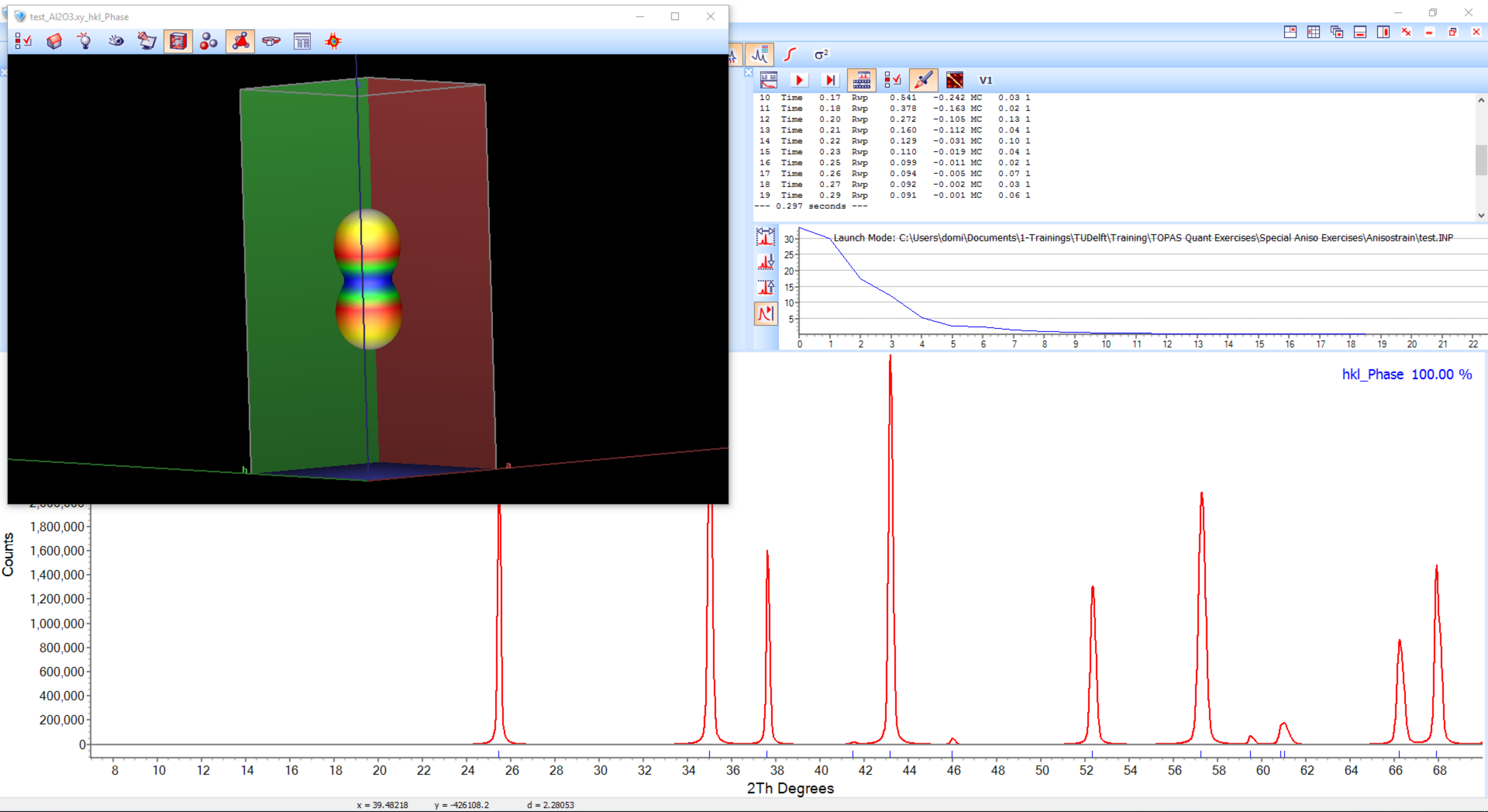

Proposed model

```
Trigonal(@  4.778000`,@  13.046004`)
AnisoST( eta, 0.00010`, ac, 0.99969`, ac, 0.99969`, cc, 2.99917`, !alc, 0, !bec, 0, !gac, 0)
```

Mixing parameter
Voigt function

a=4.778 Å±1‰

c=13.046Å±3‰

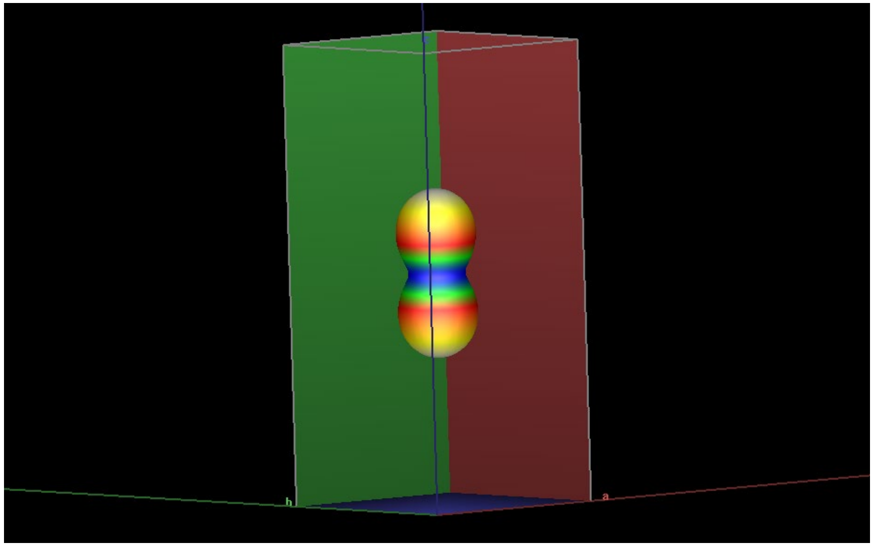

Conclusions

- *An efficient anisotropic microstrain approach for approximately linearly correlated lattice parameter distributions is presented*

- *Looking forward to see you at EPDIC 17 in 2021 and at the TOPAS User meeting*

What’s new in XRD
DISCOVER plus

D8 DISCOVER Plus
Premium Class X-ray Diffraction Solution

D8 DISCOVER Plus
Solid Foundation of **ATLAS**

Vertical θ/θ configuration
- Horizontal sample handling
- More options for sample stages

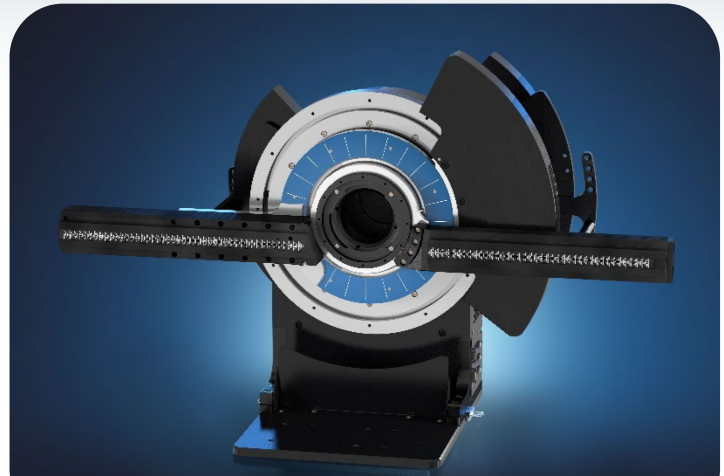

ATLAS for Sealed Tube and IμS

Based on proven D8 goniometer
- Long lifetime
- Maintenance-free

Enhanced to support R&D
- Enhanced load capability
- Enhanced mechanical stability
- Enhanced Accuracy Guarantee
  - $\Delta 2\theta \leq \pm 0.007^{\circ}$

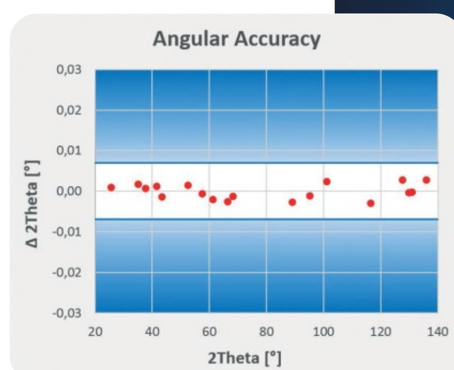

ATLAS for TXS-HE

D8 DISCOVER Plus
Benefit of ATLAS goniometer

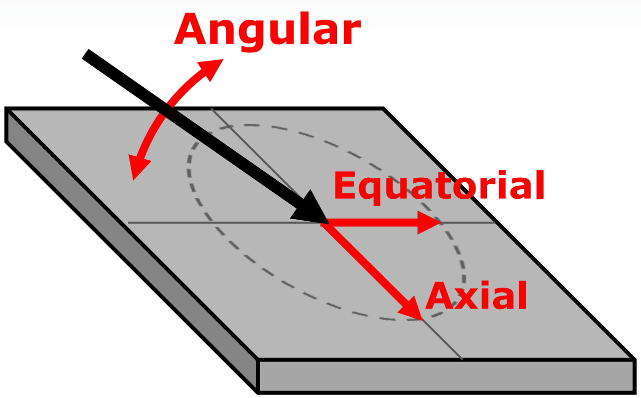

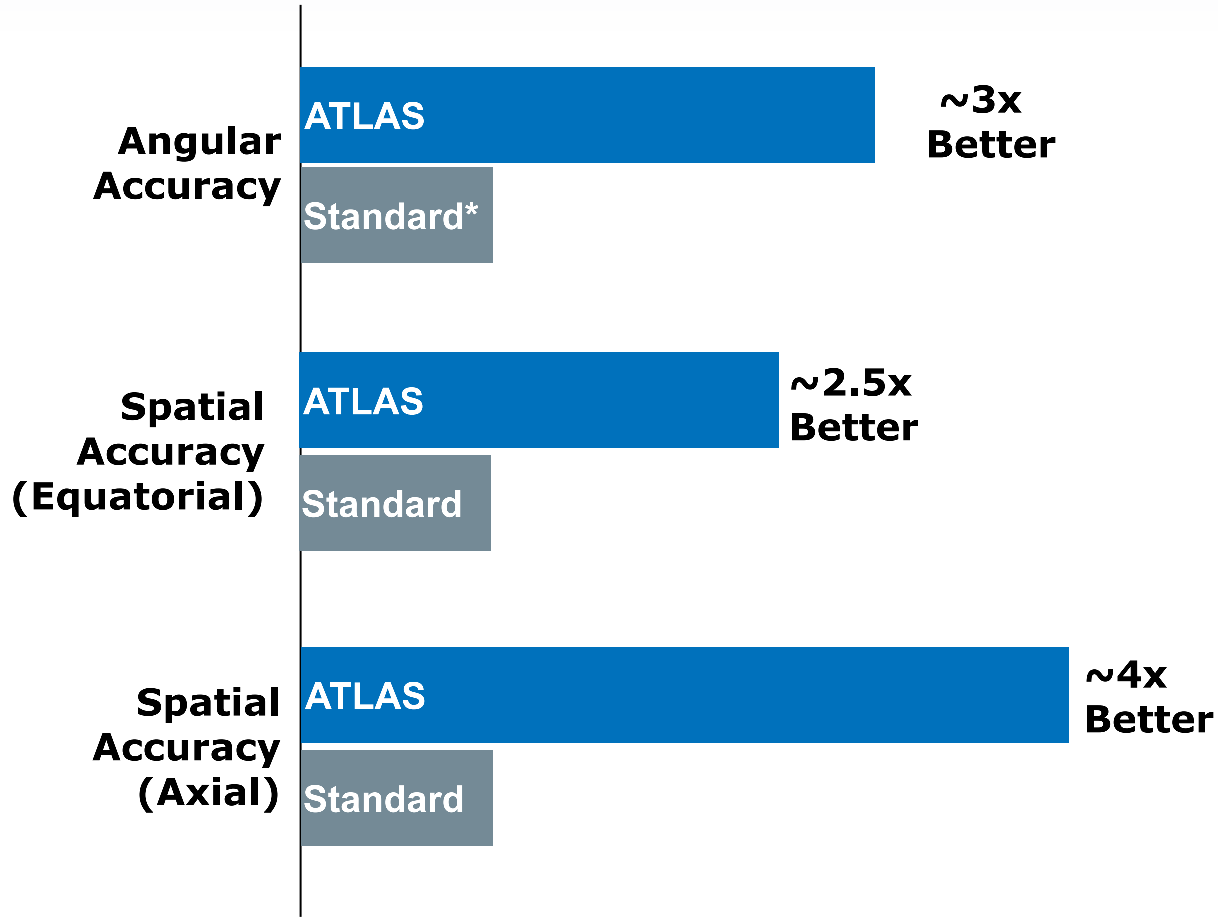

Alignment Guarantee

All NIST 1976x Peak Position

Standard D8 Goniometer

$\Delta 2\theta \leq \pm 0.01^\circ$ (for 150mm height)

$\Delta 2\theta \leq \pm 0.02^\circ$ (for 258mm height)

ATLAS Goniometer

$\Delta 2\theta \leq \pm 0.007^\circ$ (for 258mm height)

* Standard vertical D8 Goniometer

D8 DISCOVER Plus
Premium Class X-ray Diffraction Solution

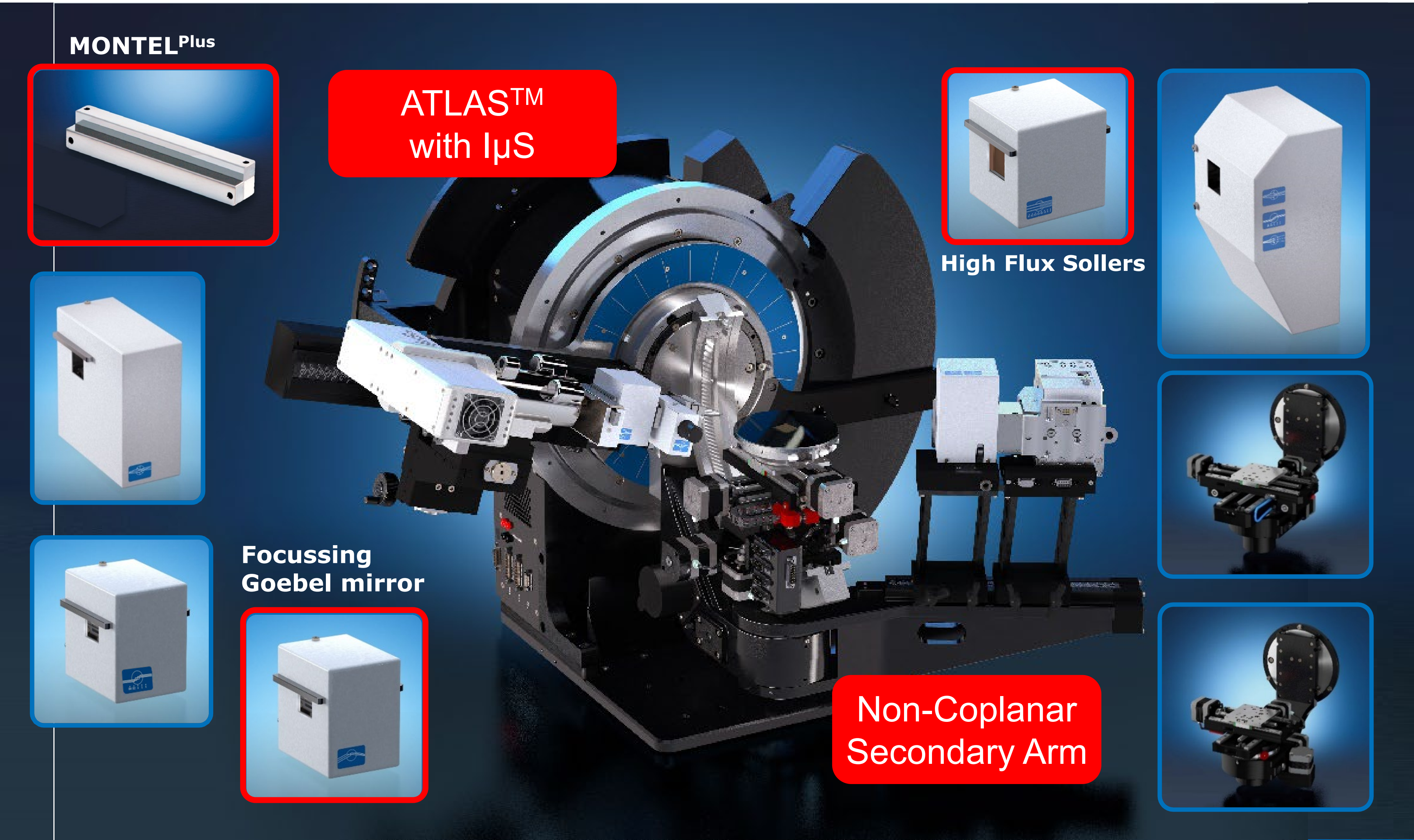

D8 DISCOVER Plus
Innovative IµS beampath for IP-GID

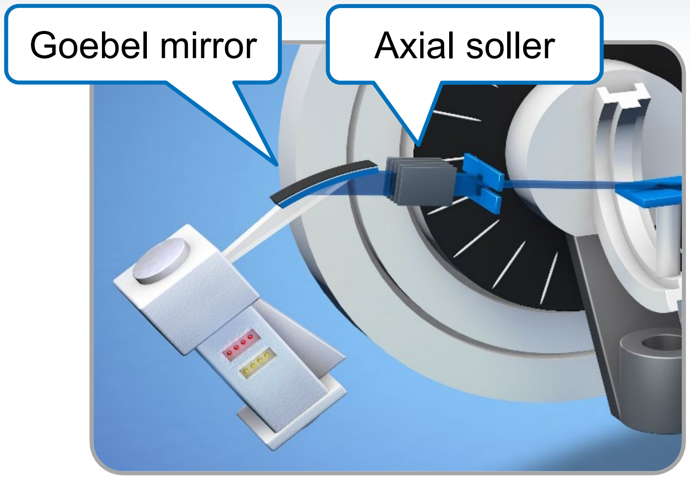

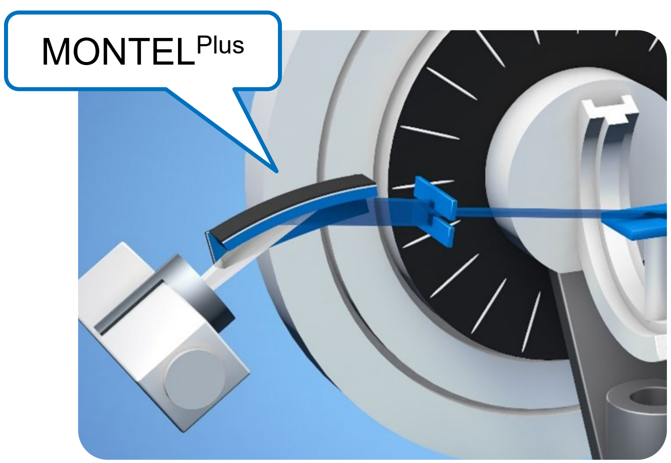

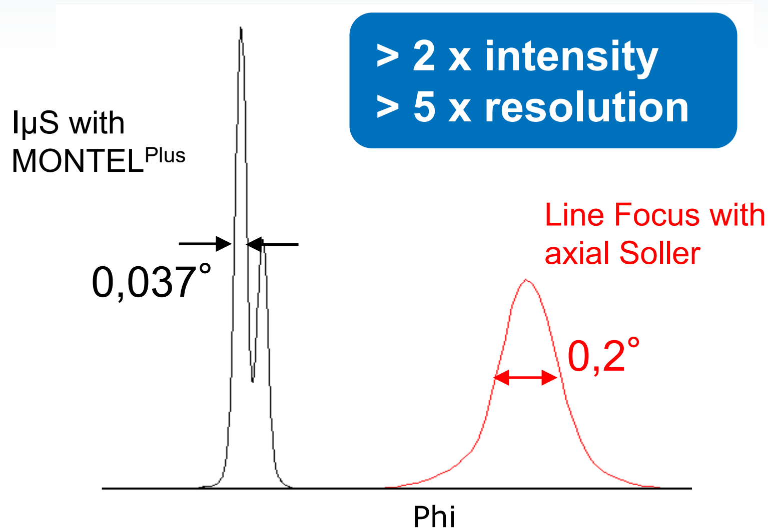

- IµS with MONTEL^{Plus} has an **exceptional In-Plane resolution** of <0,039° .
- IµS solution can be **more intense** than line focus setups.

D8 DISCOVER Plus

Innovative IµS beampath for IP-GID

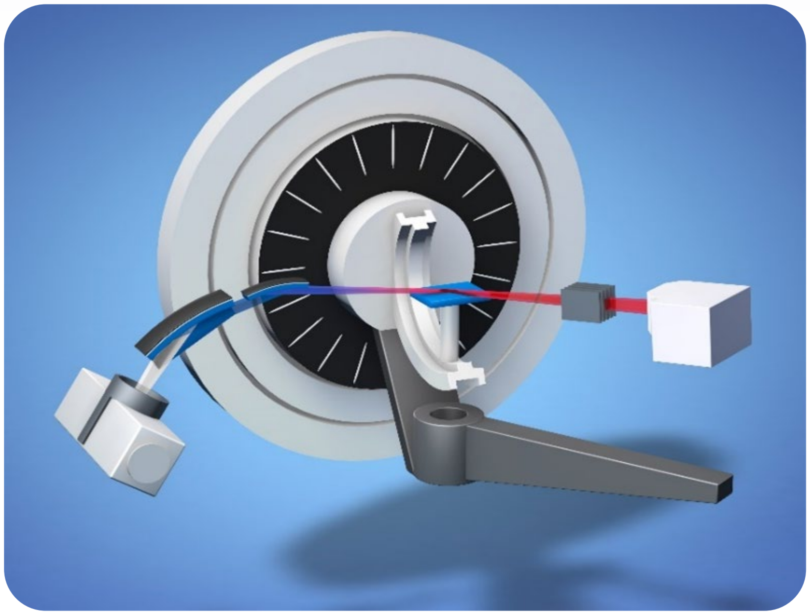

MONTEL$^{\text{Plus}}$

- Longer optics
- > 2 x intensity

Focusing Mirror

- Increased flux density
- 2-3 x intensity

High Flux Sollers

- Larger Field of View
- 2 x intensity

Total solution:
> 8 x intensity

D8 DISCOVER Plus
X-ray diffraction beyond expectations

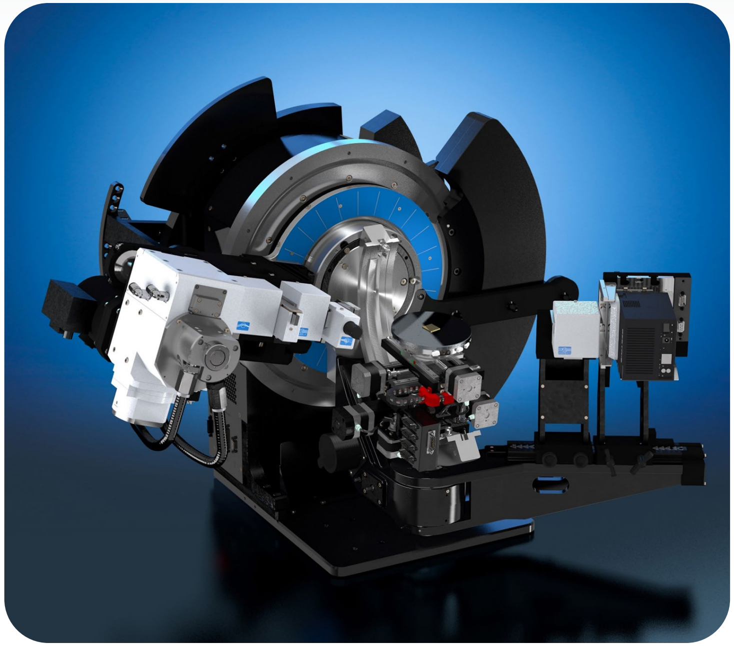

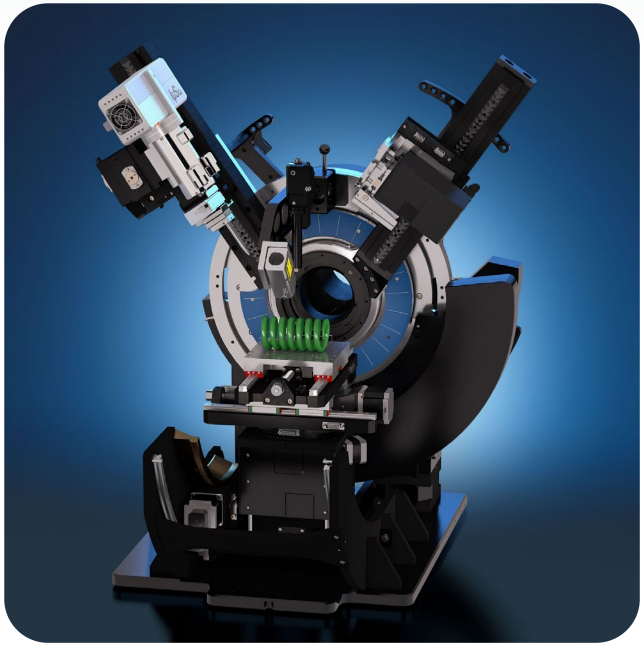

- Combining the most accurate goniometer with leading-technology X-ray sources, detectors and components to exceed your expectations.
- For further information visit us at www.bruker.com or contact your local Bruker AXS representative

Structural Characterization of ultra-thin metal films using coplanar and non-coplanar grazing incidence diffraction

Hugues Guerault
Head of Applications

Outline

- Challenges in thin film diffraction - Hardware requirements
- Benefits of wide angular scanning range
- Structural model for the refinement of thin film data

Challenges in Thin Film Diffraction
Focus on the Film

Grazing Incidence Diffraction (GID)
- Layer signal emphasized
- Substrate signal minimized

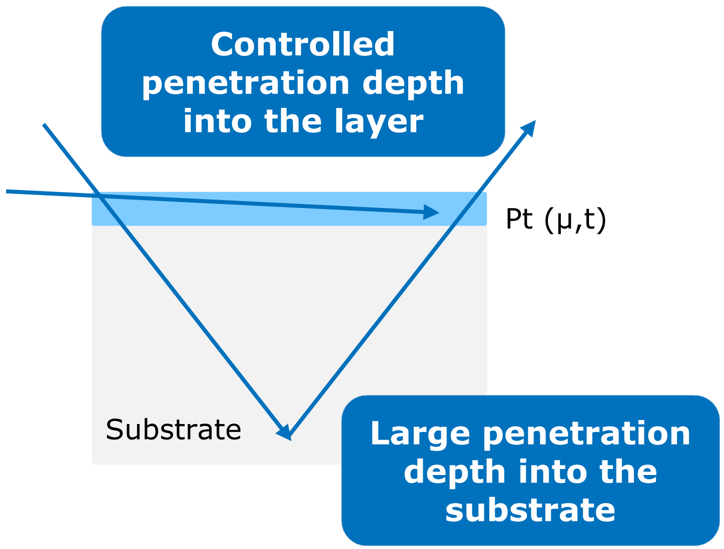

Symmetric diffraction (θ/θ)
- Low contribution from layer
- Substrate signal dominant

Diffracted intensity in symmetric diffraction

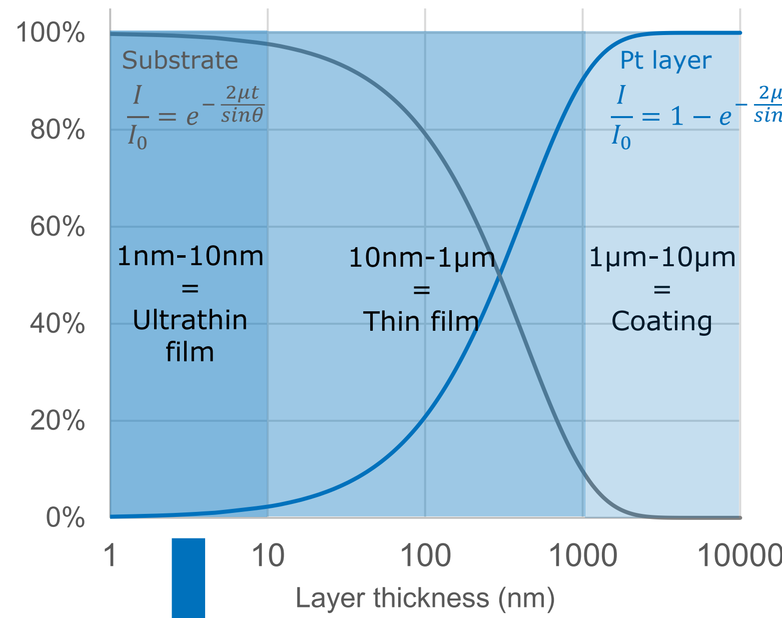

Intensity loss ≈ 2 orders of magnitude

Challenges in Thin Film Diffraction
Hardware Requirements

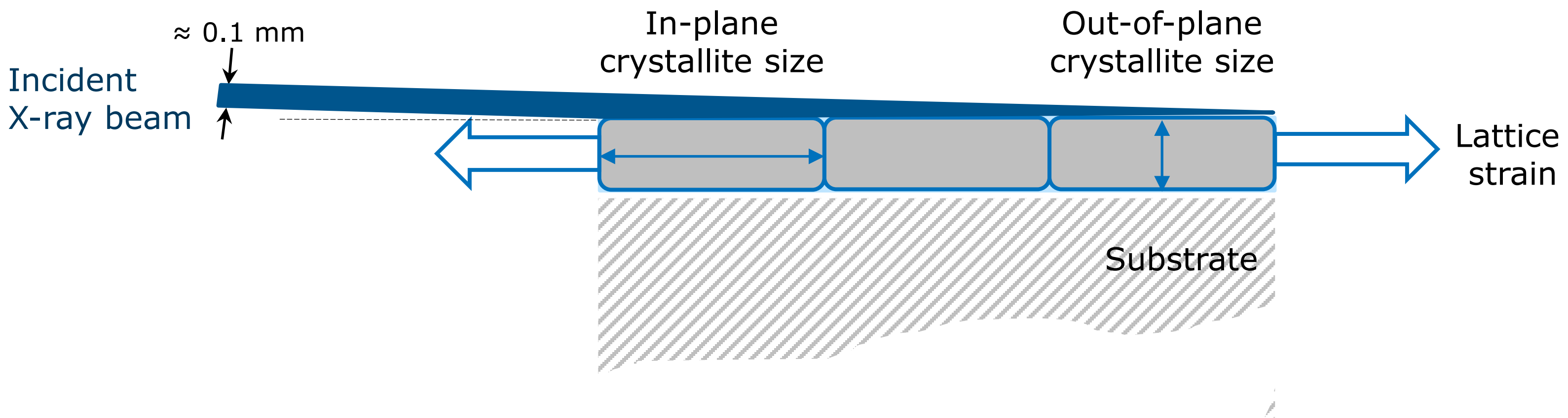

Compounding issues

- Low grain statistic (weak signal)
- Beam conditioning (reduced flux)

Need for X-ray components delivering high flux density

Anisotropic film properties

- Anisotropic crystallite shape
- Anisotropic strain

Need for goniometer accessing specific diffraction geometries

D8 DISCOVER Plus - Thin film analysis
ATLAS™ Goniometer w/ Non-Coplanar Arm

Specification Table [1]	ATLAS w/ NC	
	Coplanar	Non-Coplanar
Number of Axes	3	
Goniometer to beam [mm]	258	
Angular Range [°]	-5, … . +150	-3, … . +150
Minimum Stepsize [°]	0.0001	0.001
Max. Scan Speed [°/min]	400	360
Max. Detector Distance [mm]	370	
Detector Distance Recog	Yes	
Counterweight	Dual + ATC	
Compatible Sources	ST, IμS, TXS-HE	
Global Angular Accuracy [°]	±0.007	±0.015
Reproducibility [°]	0.0002	0.0002

[1] Specifications dependent on absolute configuration

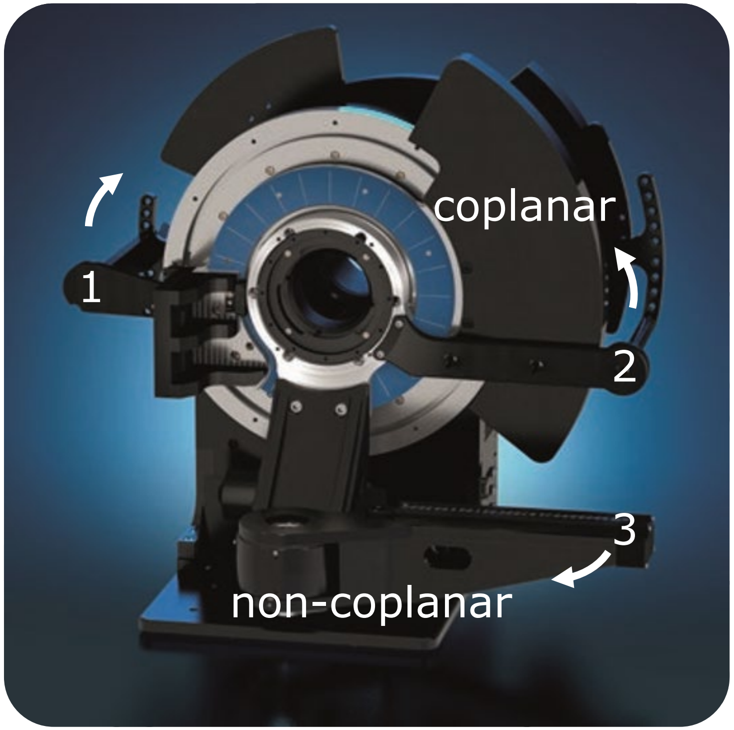

D8 DISCOVER Plus - Thin film analysis
High Flux Components

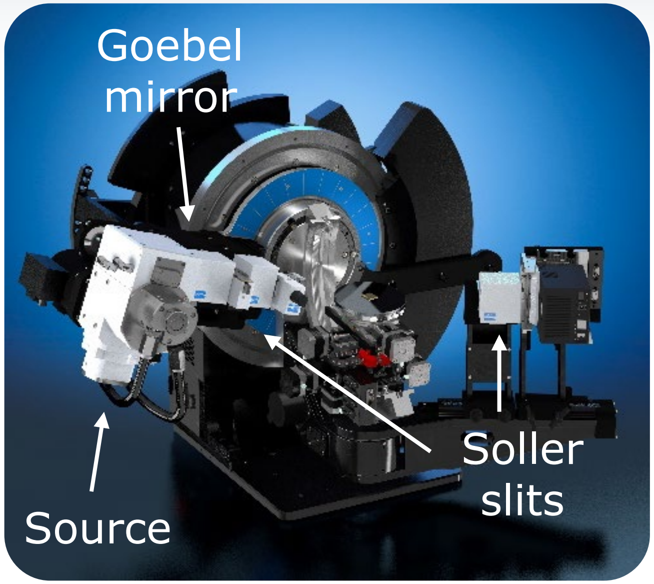

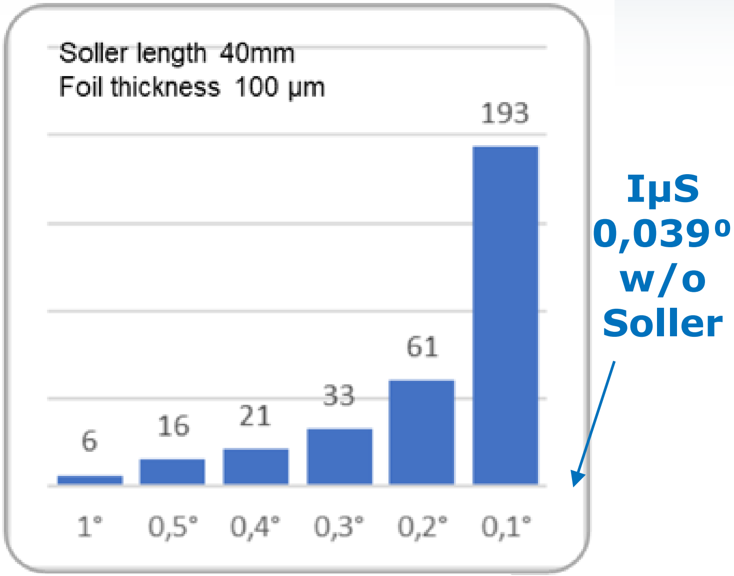

Intensity loss factor of axial Soller slit

X-ray source

- IµS for best IPGID resolution
- Ceramic sealed tube
- Rotating anode generator

x5

Primary beam conditioning

- Parallel beam Goebel mirror
- Focusing beam Goebel mirror

x3

Soller slits

- Adjust resolution to sample
- For ultrathin films favor flux rather than resolution

Phase Analysis
10 nm Pt on Glass

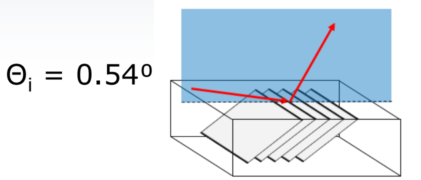

Coplanar GID

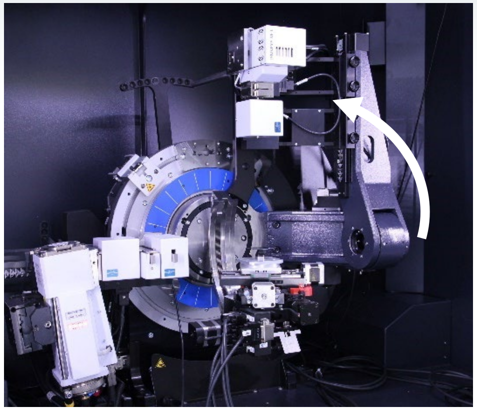

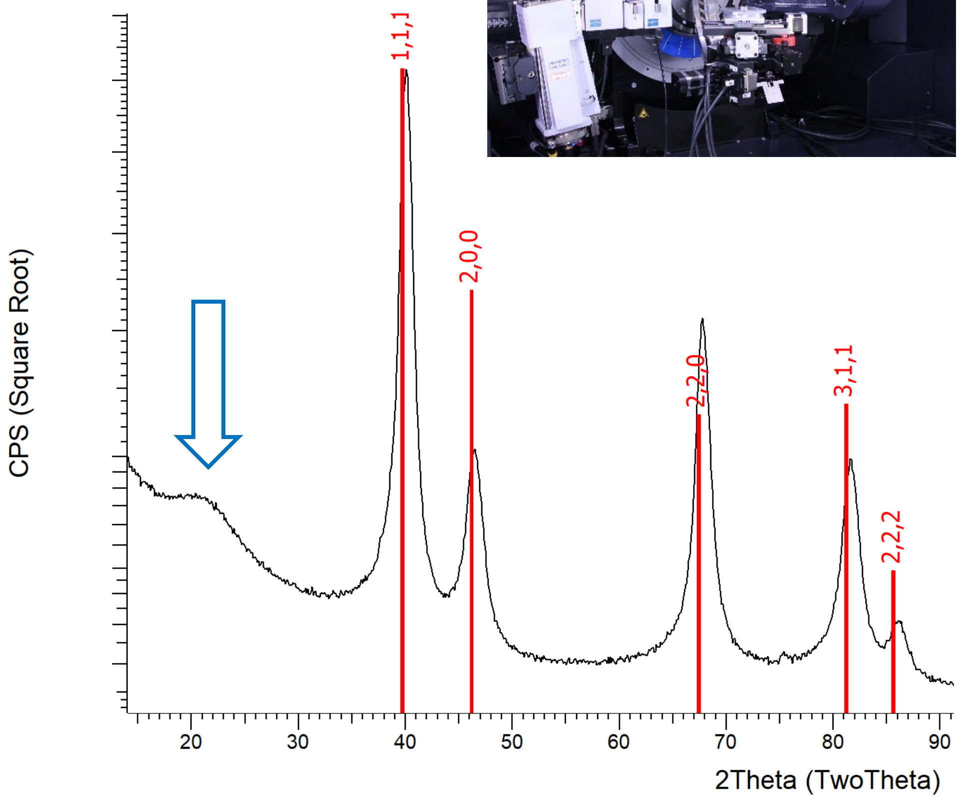

Slight peak shift due to refraction at sample surface

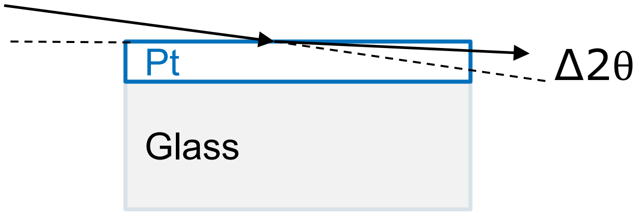

After offset correction

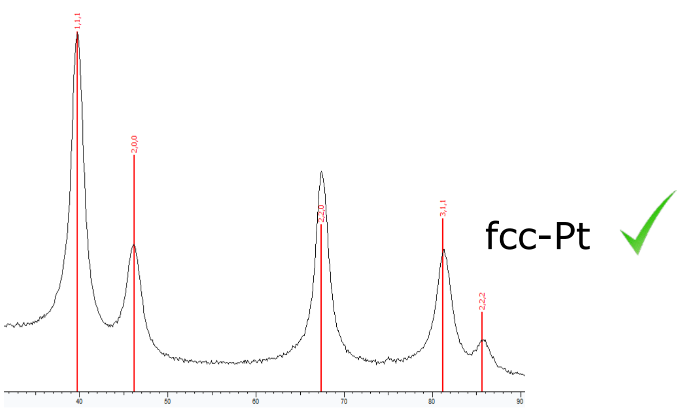

Extended Scan Range

10 nm Pt on Glass

$\Theta_i = 0.54^o$

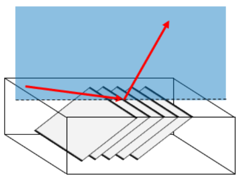

Coplanar GID

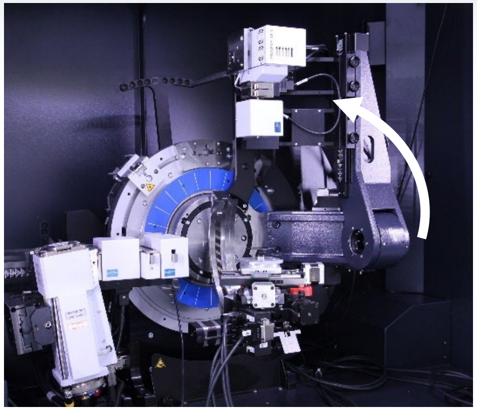

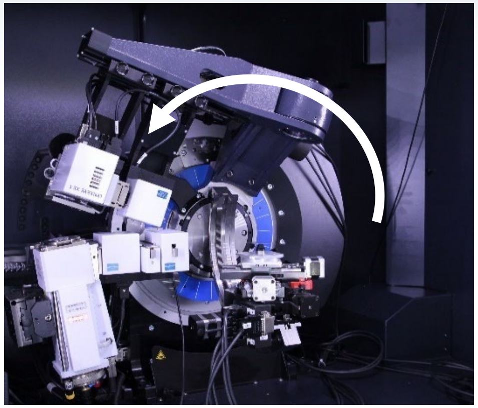

Angular dependent peak shift
=
Residual Stress

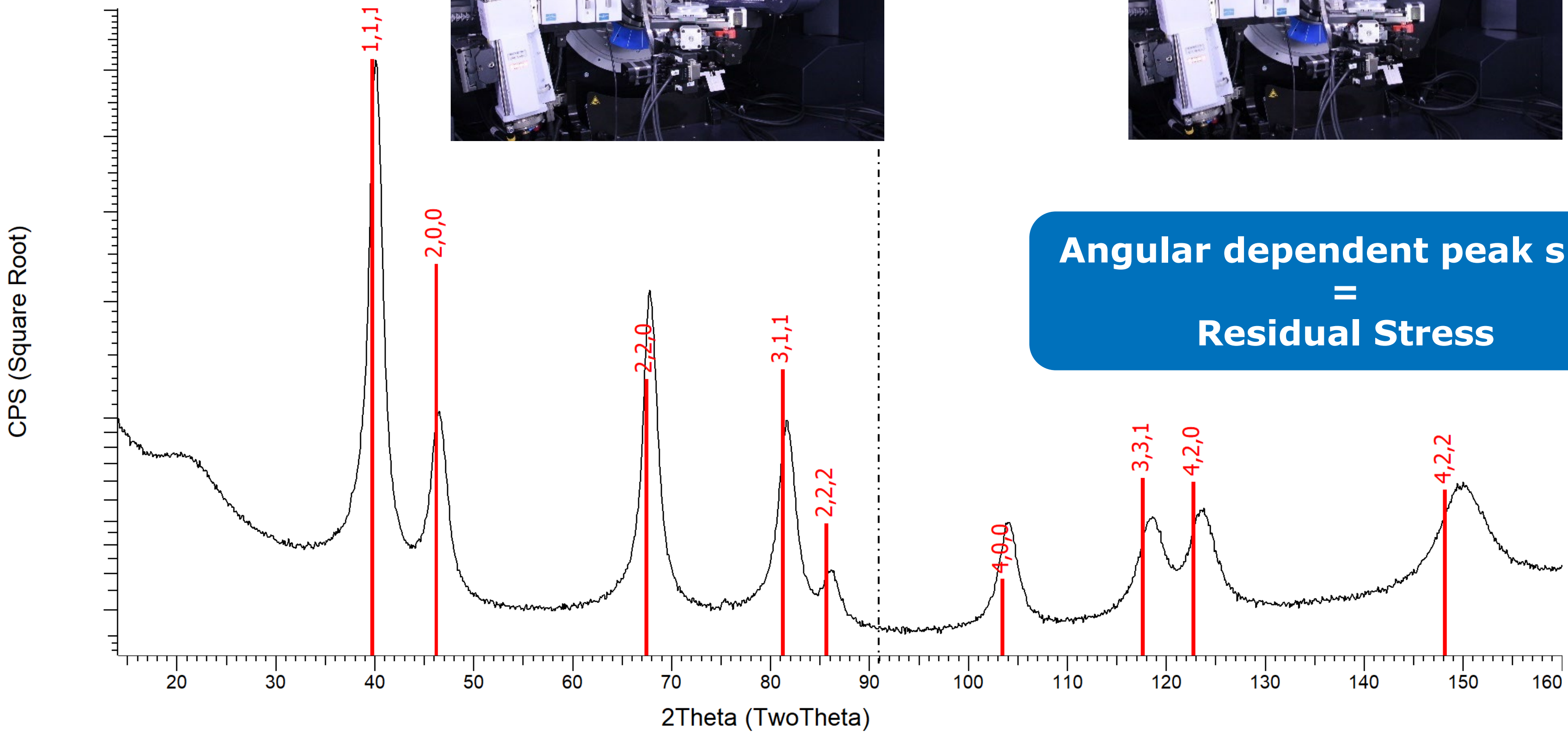

Why Do High Angle Data Matter?

Structural Parameters

Angular shift due to residual stress

$$\Delta 2\theta = -\frac{2\,\sigma\,tan\theta}{E}\left((\nu+1)\,sin^2\psi\ - 2\nu\right)$$

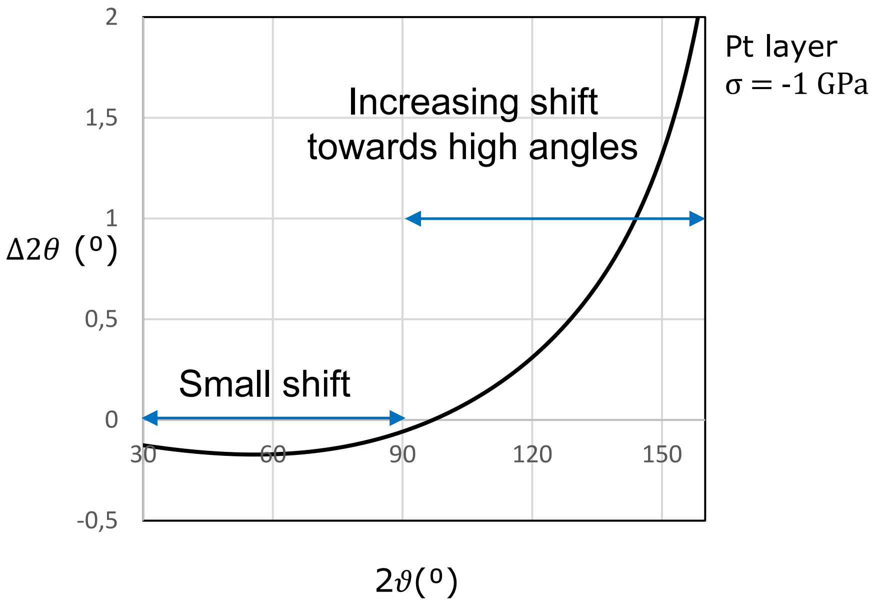

Accuracy on lattice parameter

$$d = \frac{\lambda}{2\,sin\theta} \Rightarrow \frac{\delta d}{d} \sim cotan\vartheta\,\delta\vartheta$$

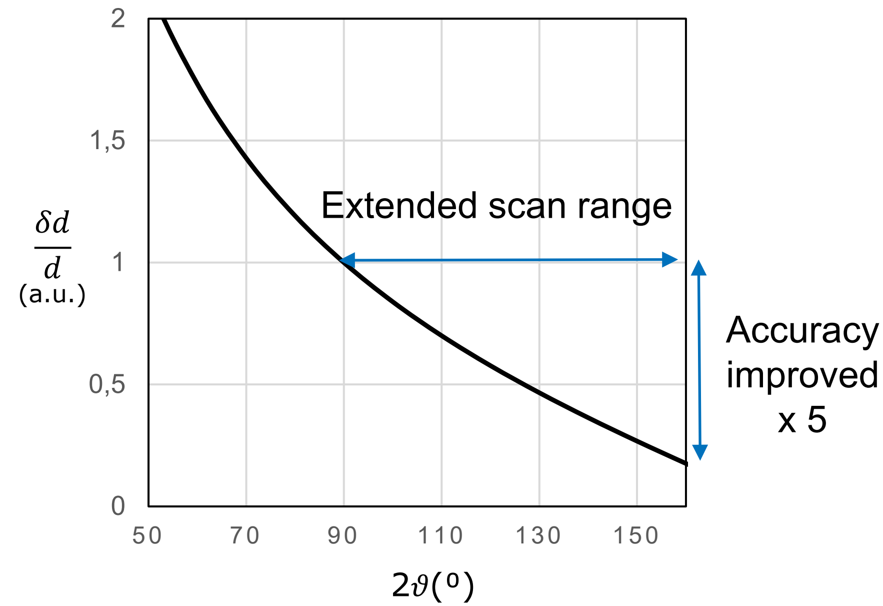

- **Wide angular range essential in residual stress analysis**
- **High angle data improves lattice parameter accuracy (x5)**

Why Do High Angle Data Matter?
Microstructural Parameters

Accuracy on crystallite size L

$$L = \frac{k\lambda}{\beta_L \cos\theta} \Rightarrow \frac{\delta L}{L} = \frac{\partial \beta_L}{k\,\lambda} L \cos\vartheta + \tan\theta\,\delta\theta$$

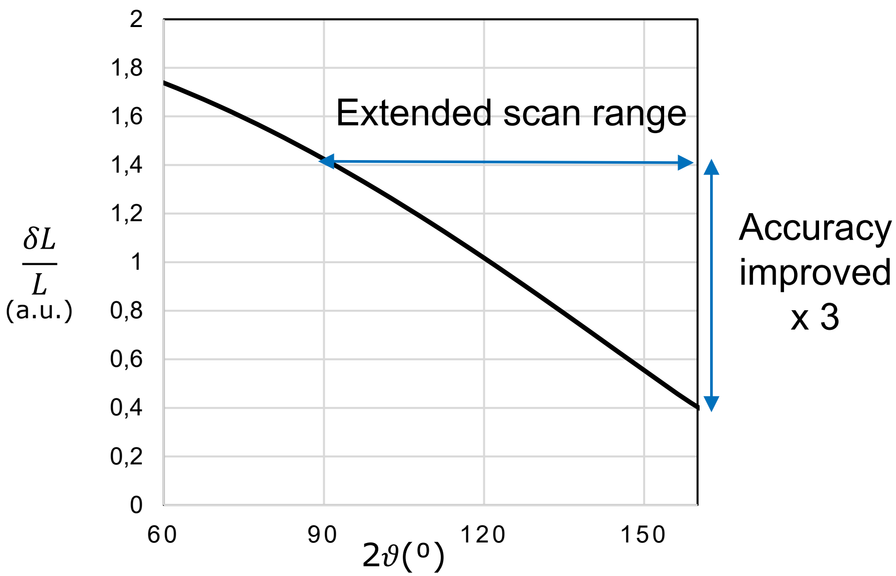

L=15 nm

Accuracy on microstrains ε

$$\varepsilon = \frac{\beta_\varepsilon}{4\tan\theta} \Rightarrow \frac{\delta\varepsilon}{\varepsilon} = \frac{\delta\beta_\varepsilon}{4\,\varepsilon\tan\theta} + \frac{2\,\delta\vartheta}{\sin(2\vartheta)}$$

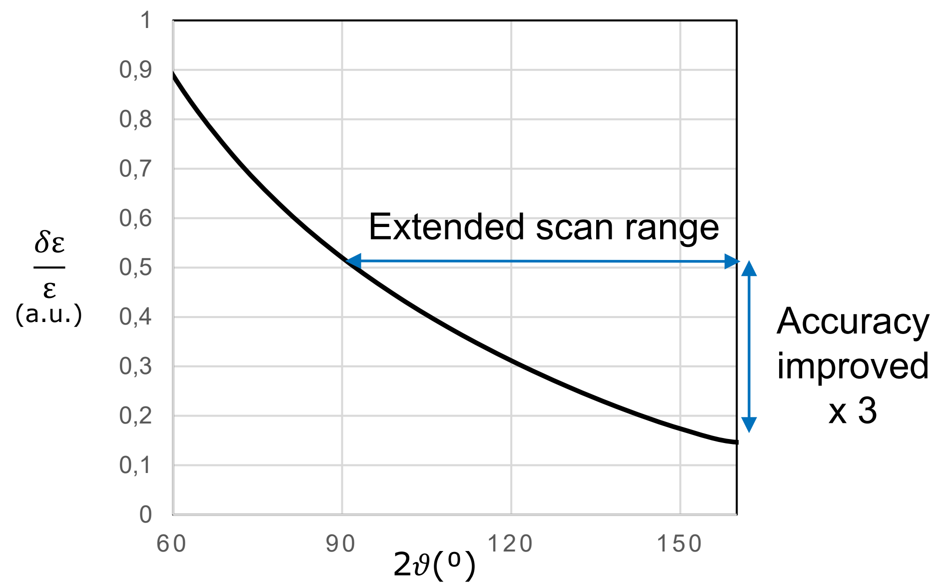

ε=0,5%

- **Wide angular range = better Size/Strain deconvolution**
- **High angle data improve microstruture accuracy (x3)**

Non-Coplanar Arm
A Wide Angular Range

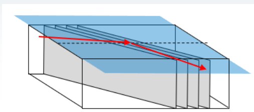

Non-coplanar GID

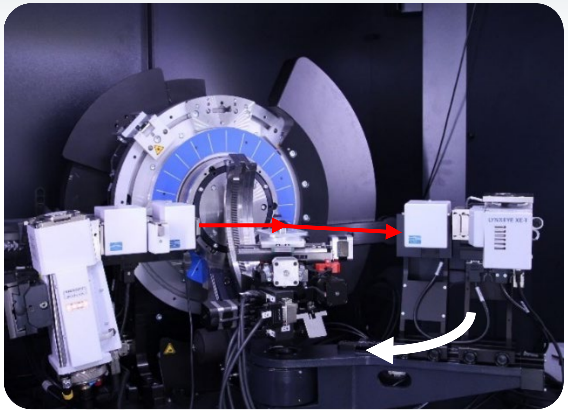

Front view – Intermediate angle

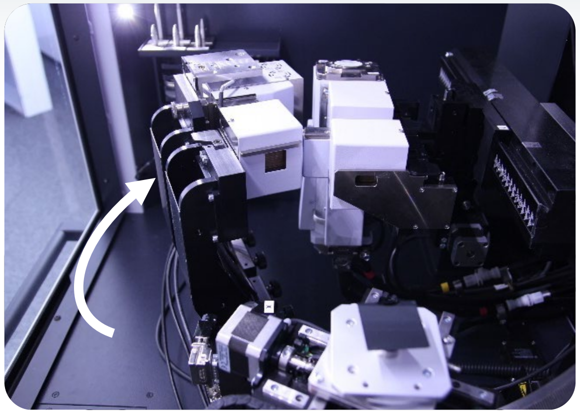

Top view – Highest angle

Coplanar vs Non-coplanar
Unconsistent peak positions

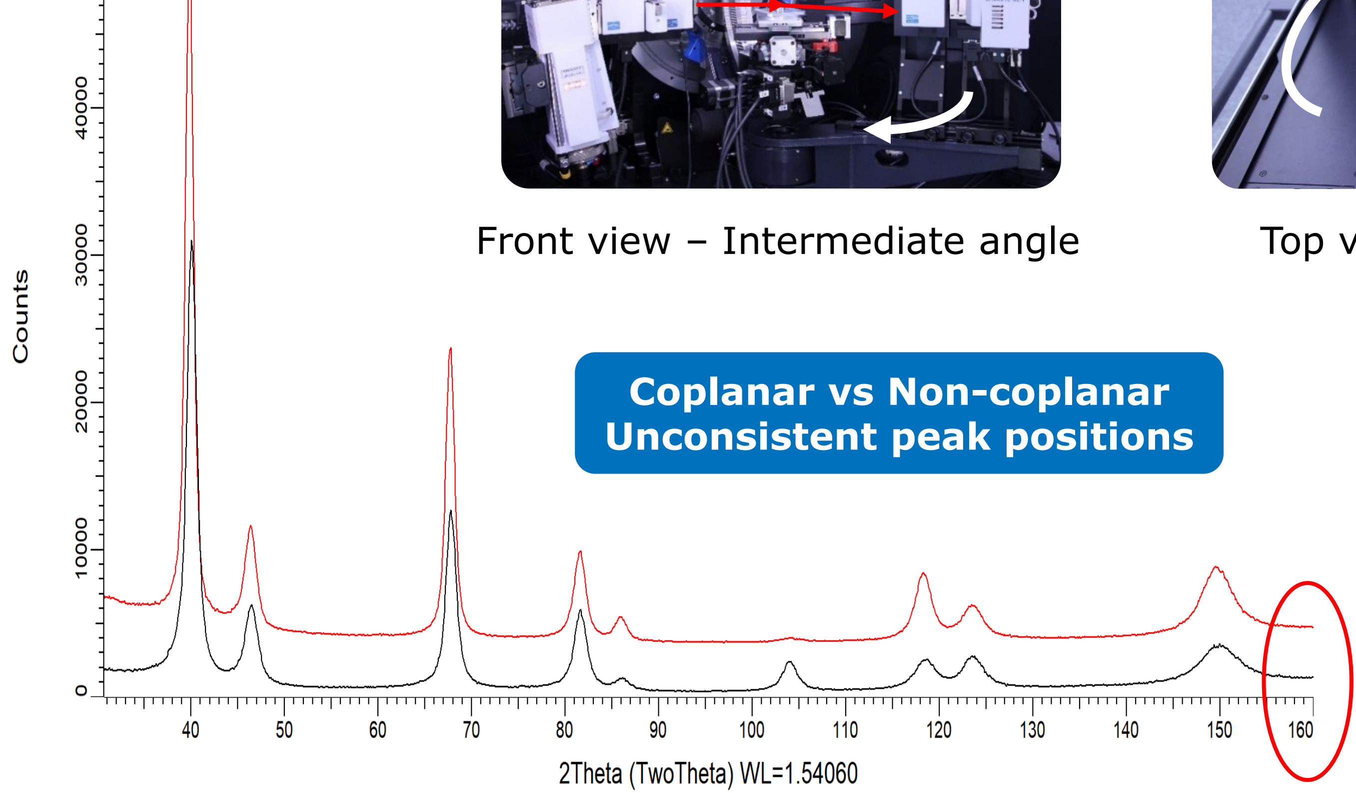

non-coplanar (2 hours)
0,5 º Soller / 1º Soller

coplanar (2 hours)
No Soller / 1º Soller

Data Refinement in TOPAS
Structural model

- Coplanar and non-coplanar data **refined simultaneously with unique model**

Parameters	GID	IPGID
Lattice constant	a_0 (stress free)	$a_0 + \frac{1-\nu}{E}\sigma$
2θ shift from residual stress	$-\frac{2\,\sigma\,\tan\theta}{E}\left((\nu+1)\sin^2\psi - 2\nu\right)$	
2θ shift from refraction	$\theta_i - \sqrt{\theta_i^2 - \theta_c^2}$	
Crystallite size	L_{OP}	L_{IP}
Microstrains	ε	

θ_i *incident angle*

$\psi = 2\theta - \theta_i$

Material constants

θ_c *critical angle*
ν *Poisson ratio*
E *Young modulus*

5 physical parameters
$a_0,\ \sigma,\ L_{OP},\ L_{IP},\ \varepsilon$

Data Refinement in TOPAS
10 nm Pt on Glass

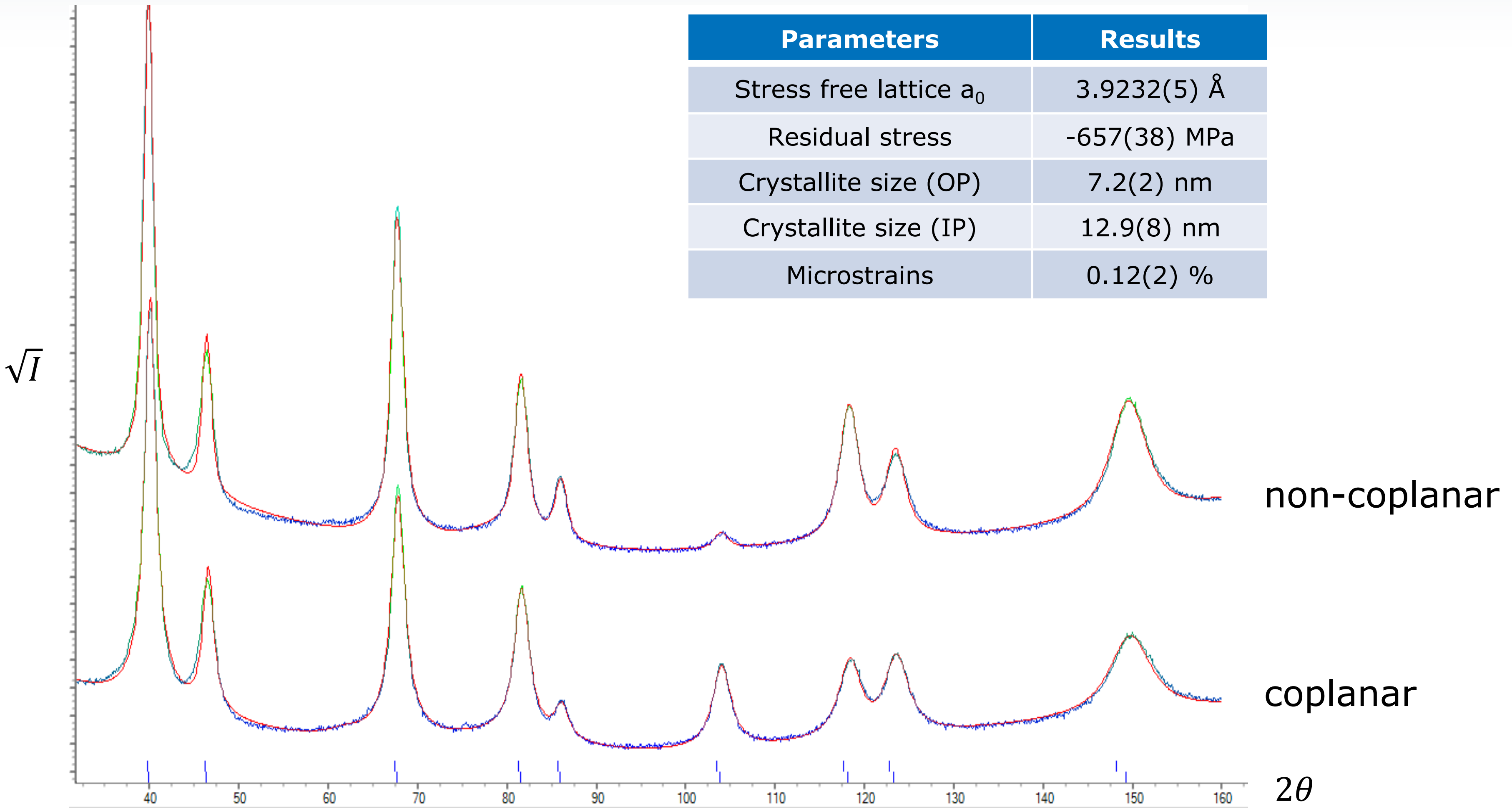

Parameters	Results
Stress free lattice a_0	3.9232(5) Å
Residual stress	-657(38) MPa
Crystallite size (OP)	7.2(2) nm
Crystallite size (IP)	12.9(8) nm
Microstrains	0.12(2) %

Summary

- **D8 DISCOVER Plus** offers complete solutions for the analysis of (ultra)-thin polycrystalline films
- **ATLAS™ Goniometer** acquires accurate data on a **wide angular range** for best evaluation results
- Data from both coplanar and non-coplanar geometries are refine simultaneously in **TOPAS** using a **unique structural model**

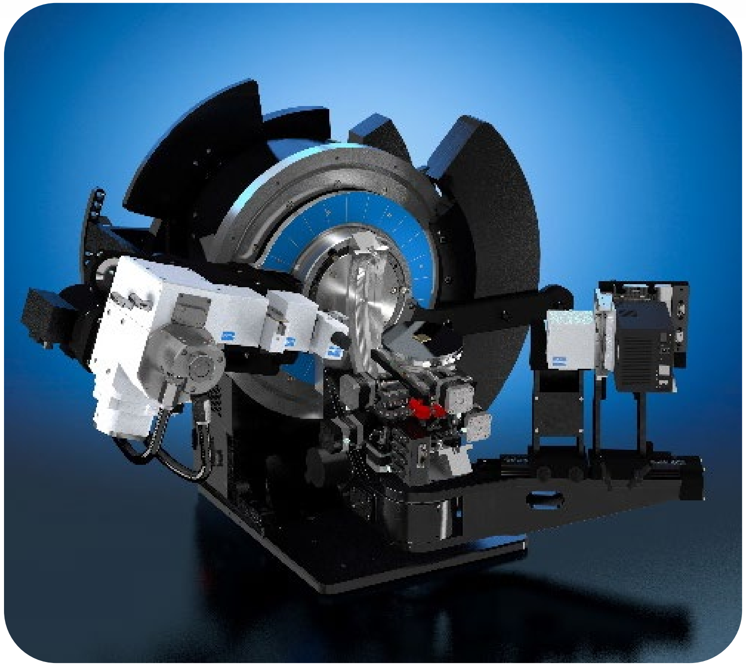

D8 DISCOVER Plus
w/ non-coplanar arm

Application of Deep Learning to XRD Phase Identification

Jan Schützke[1,2], Ralf Mikut[1], Alexander Benedix[2], Karsten Knorr[2] & Markus Reischl[1]

1. Institute for Automation and Applied Informatics, KIT, Karlsruhe, Germany;
2. Bruker AXS GmbH, Karlsruhe, Germany

Jan Schützke
PhD student

Motivation
Fast and objective analysis

Problem:

- Manual Phase Identification (qualitative analysis) for powder XRD scans
  - Require expertise
  - Time-consuming
  - Error prone
  - Not objective (possibly differing results for identical scan)

→ Automation of phase identification analysis

Concept

Automatic Phase Identification

- Instead of hard-coding all analysis criteria and methods:
  Use of trainable approach (Machine learning algorithm)

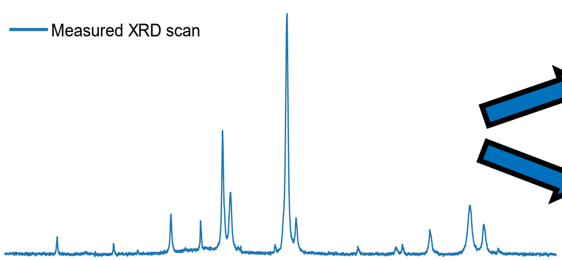

conventional approach

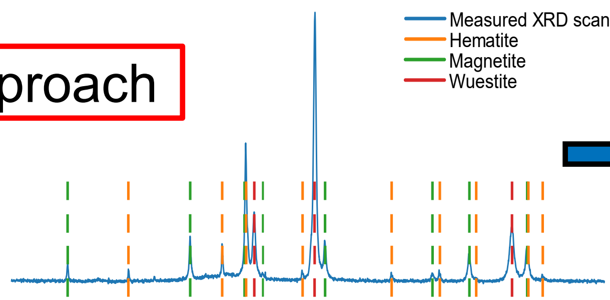

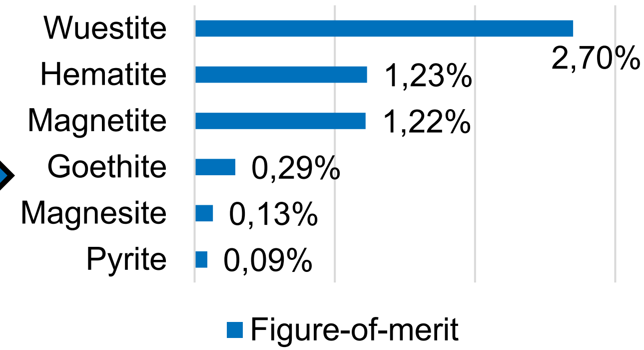

new approach

Automatic approach

Phase	Output
Wuestite	✓
Hematite	✓
Magnetite	✓
Magnesite	×
Talc	×

- Desired output of automatic phase identification is binary:
  1 for present and 0 for absent phases

Simulation of XRD Scans
Generating Training Data

- Training process of machine learning algorithm requires thousands of samples
- Not enough measured and labelled samples available

➡ Simulation of powder XRD scans for training purposes

- Generation of synthetic diffraction patterns through TOPAS
- Mixing of phases with random weight percentages
- Synthetic scan includes background (high-order polynomial function), Gaussian noise and additional effects like air scattering

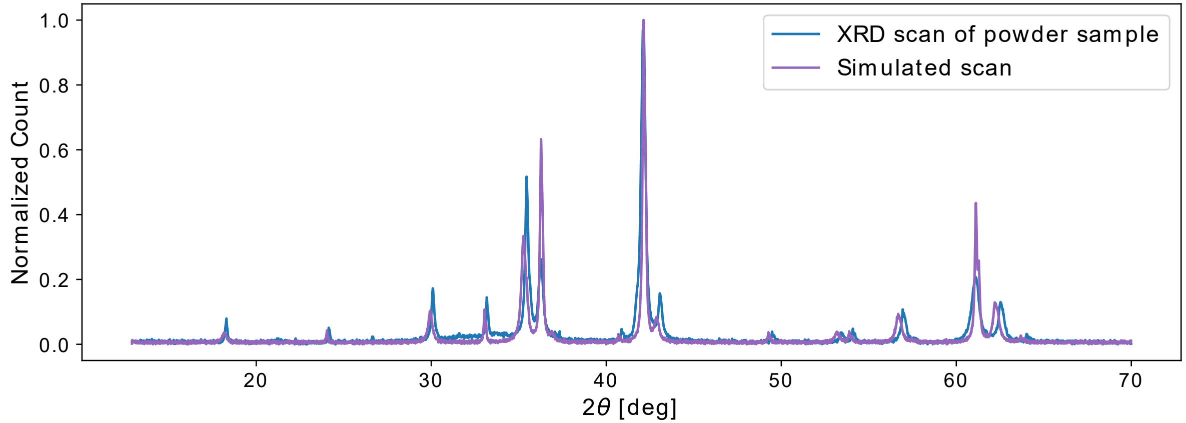

Application Packages
Arranging Training Sets

- Identification of application packages:
  Automatic approach applicable for all phases *but* performs better for a limited number of candidate phases (shown in the results)

- We evaluate the performance for 2 application packages:
  1. Iron ore samples with 28 possible phases
  2. Cement samples with 76 candidate phases

- Generation of *500,000* synthetic mixture scans for training and additional *100,000* validation samples
- Supplementary information for each training sample with target output: 1 for present phases, 0 for absent phases in the mixture

Neural Networks
Structure and Functionality

- Usage of *neural networks* for automatic phase identification approach
- Input: Raw scan as 1D image
- Identical 2Θ range and Δ2Θ required!
- Here: 5° to 70° with 0.01 Δ2Θ
  ➡ 6500 datapoints
- Output: Certainty score (0-1) for presence of each phase

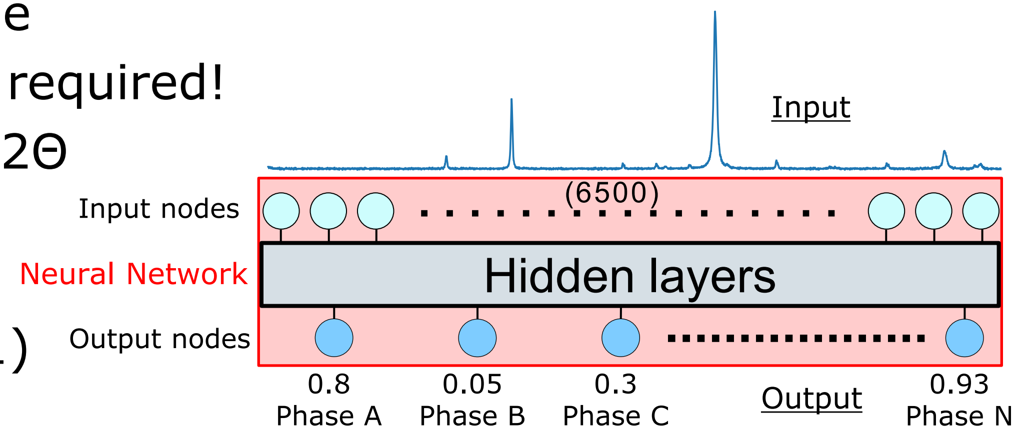

- Training of network by optimizing the binary cross-entropy:
  - Propagation of raw scan through network, receiving output
  - Calculation of binary cross-entropy by comparing actual to target output
  - Adaption of weights in hidden layer by backpropagation

Results

Application Package	Candidates	Accuracy (False-to-Total Ratio)	False-to-Positives Ratio
Iron Ores	28	99.99%	99.54%
Cements	76	99.99%	98.60%
Combination	345	99.99%	91.30%

- We achieve an accuracy of nearly 100% for all tested application packages (iron ores and cements)
- After further evaluation: *More False Positives* and *False Negatives* for packages with *greater number of candidates*
- Performance validated with measured scans
- Comparison with an expert: Network identifies more phases but also finds more False Positives ➡ *close to human performance*
- Network model analyzes hundreds of scans per second

- Outlook: One classifier for larger application packages

Questions and Answers

Thank you for joining this luncheon!

Fee free to ask your questions now or contact your local Bruker representative later.

We look forward meeting you at the EPDIC conference in 2021 and at the TOPAS users meeting. Stay well!

Karsten Knorr

Product Manager
Industrial XRD

Innovation with Integrity